

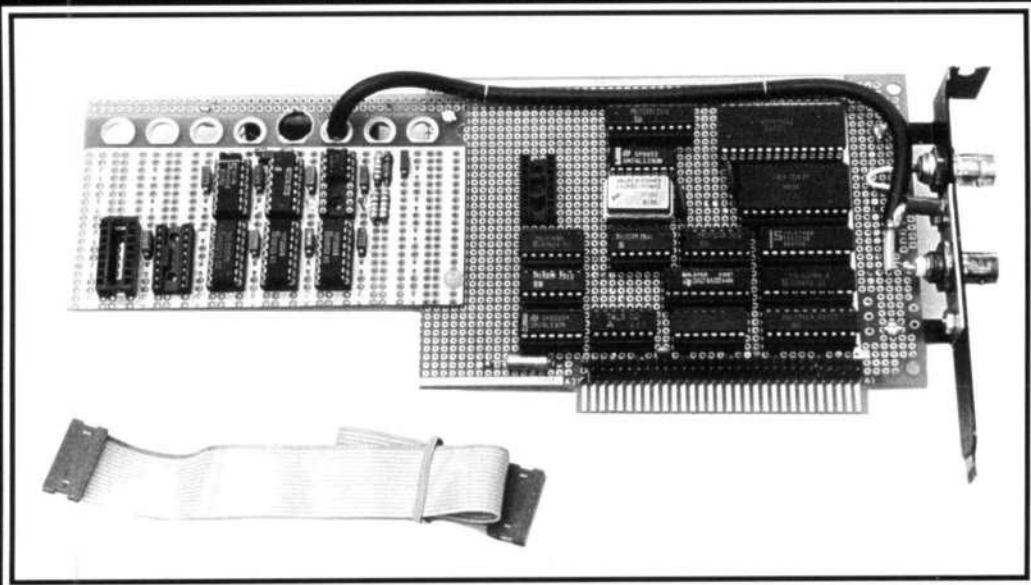
QEX

\$1.75



ARRL Experimenter's Exchange

January 1994



A Frequency Counter for Your PC

QEX: The ARRL
Experimenter's Exchange
American Radio Relay League
225 Main Street
Newington, CT USA 06111

QEX

QEX (ISSN: 0886-8093) is published monthly by the American Radio Relay League, Newington, CT USA.

Application to mail at second-class postage rates is pending at Hartford, CT.

David Sumner, K1ZZ
Publisher

Jon Bloom, KE3Z
Editor

Lori Weinberg
Assistant Editor

Harold Price, NK6K
Zack Lau, KH6CP
Contributing Editors

Production Department

Mark J. Wilson, AA2Z
Publications Manager

Michelle Bloom, WB1ENT
Production Supervisor

Sue Fagan
Graphic Design Supervisor

Dianna Roy, Deborah Strzeszkowski
Senior Production Assistants

Advertising Information Contact:

Brad Thomas, KC1EX, Advertising Manager
American Radio Relay League
203-667-2494 direct
203-666-1541 ARRL
203-665-7531 fax

Circulation Department

Debra Jahnke, Manager
Kathy Fay, N1GZO, Deputy Manager
Cathy Stepina, QEX Circulation

Offices

225 Main St, Newington, CT 06111-1494
USA
Telephone: 203-666-1541
Telex: 650215-5052 MCI
FAX: 203-665-7531 (24 hour direct line)
Electronic Mail: MCIMAILID: 215-5052
Internet: qex@arrl.org

Subscription rate for 12 issues:

In the US: ARRL Member \$12,
nonmember \$24;

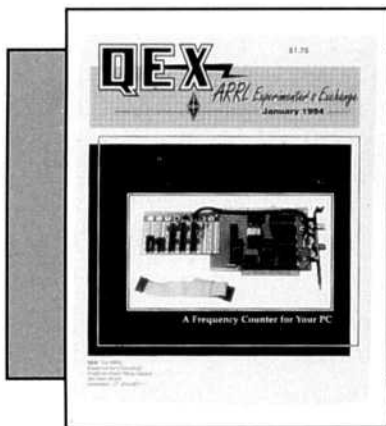
US, Canada and Mexico by First Class
Mail:
ARRL Member \$25, nonmember \$37;

Elsewhere by Airmail:
ARRL Member \$48, nonmember \$60.

QEX subscription orders, changes of address, and reports of missing or damaged copies may be marked: QEX Circulation. Postmaster: Form 3579 requested. Send change of address to: American Radio Relay League, 225 Main St, Newington, CT 06111-1494.

Members are asked to include their membership control number or a label from their QST wrapper when applying.

Copyright © 1993 by the American Radio Relay League Inc. Material may be excerpted from QEX without prior permission provided that the original contributor is credited, and QEX is identified as the source.



About the Cover:

This design by NS6Z provides 0-1 GHz frequency measurement for your PC.

ISSUE
NO.
143



Features

3 Personal Computer Frequency Counter

By John Nemece, NS6Z

9 All About Phase Noise in Oscillators

Part 2 of 3

By Ulrich L. Rohde, KA2WEU

17 Digital Processing of Weak Signals Buried in Noise

By Darrel Emerson, AA7FV/G3SYS

Columns

26 RF

By Zack Lau, KH6CP/1

29 Upcoming Technical Conferences

January 1994 QEX Advertising Index

AMSAT: 28
American Radio Relay League:
25, 30, 31
Communications Specialists Inc: 25
Down East Microwave: 8
Henry Radio: Cov III
L.L. Grace: Cov II

LUCAS Radio/Kangaroo Tabor
Software: 28
Mike Cook, AF9Y: 30
P.C. Electronics: 31
Tucson Amateur Packet Radio Corp: 30
Yaesu: Cov IV
Z Domain Technologies, Inc: 25

THE AMERICAN RADIO RELAY LEAGUE



The American Radio Relay League, Inc. is a noncommercial association of radio amateurs, organized for the promotion of interests in Amateur Radio communication and experimentation, for the establishment of networks to provide communications in the event of disasters or other emergencies, for the advancement of radio art and of the public welfare, for the representation of the radio amateur in legislative matters, and for the maintenance of fraternalism and a high standard of conduct.

ARRL is an incorporated association without capital stock chartered under the laws of the state of Connecticut, and is an exempt organization under Section 501(c)(3) of the Internal Revenue Code of 1986. Its affairs are governed by a Board of Directors, whose voting members are elected every two years by the general membership. The officers are elected or appointed by the Directors. The League is noncommercial, and no one who could gain financially from the shaping of its affairs is eligible for membership on its Board.

"Of, by, and for the radio amateur," ARRL numbers within its ranks the vast majority of active amateurs in the nation and has a proud history of achievement as the standard-bearer in amateur affairs.

A bona fide interest in Amateur Radio is the only essential qualification of membership; an Amateur Radio license is not a prerequisite, although full voting membership is granted only to licensed amateurs in the US.

Membership inquiries and general correspondence should be addressed to the administrative headquarters at 225 Main Street, Newington, CT 06111 USA.

Telephone: 203-666-1541 Telex: 650215-5052 MCI.

MCIMAIL (electronic mail system) ID: 215-5052 FAX: 203-665-7531 (24-hour direct line)

Officers

President: GEORGE S. WILSON III, W4OYI
1649 Griffith Ave, Owensboro, KY 42301

Executive Vice President: DAVID SUMNER, K1ZZ

Purpose of QEX:

- 1) provide a medium for the exchange of ideas and information between Amateur Radio experimenters
- 2) document advanced technical work in the Amateur Radio field
- 3) support efforts to advance the state of the Amateur Radio art

All correspondence concerning QEX should be addressed to the American Radio Relay League, 225 Main Street, Newington, CT 06111 USA. Envelopes containing manuscripts and correspondence for publication in QEX should be marked: Editor, QEX.

Both theoretical and practical technical articles are welcomed. Manuscripts should be typed and doubled spaced. Please use the standard ARRL abbreviations found in recent editions of *The ARRL Handbook*. Photos should be glossy, black and white positive prints of good definition and contrast, and should be the same size or larger than the size that is to appear in QEX.

Any opinions expressed in QEX are those of the authors, not necessarily those of the editor or the League. While we attempt to ensure that all articles are technically valid, authors are expected to defend their own material. Products mentioned in the text are included for your information; no endorsement is implied. The information is believed to be correct, but readers are cautioned to verify availability of the product before sending money to the vendor.

Empirically Speaking

Second Class Is First Class (Compared to Third Class)

If all of our plans come together, this issue of QEX will be the first one mailed via second-class mail in the US. (We're still working out the details with the Postal Service.) This issue is being mailed from Newington; future issues will come to you directly from the printing plant in Austin, Texas. Most QEX subscribers presently receive their copy via third-class mail. That class of service is, um, variable in its efficiency. The change to second-class mailing, while somewhat more expensive, will allow us to get QEX to you in a more timely manner, and with fewer problems. Those who receive QEX via first-class mail will continue to do so, and we'll continue to offer the first class option for now, but we expect that many of you will choose second class service at renewal.

The change in mailing status is accompanied by the last of our scheduled major format changes, as QEX becomes a full 32 pages each month. We're also having the magazine printed on a new type of paper. With these changes, we bring to a close our year-plus-long effort to remake QEX. As we said in this space last month, it's now up to you to supply the articles to fill the new QEX!

How Technical Is "Too Technical"

I've had a bit of feedback about the series we're currently running, about phase noise. Some readers seem to feel it's "too technical," or at least over their heads. We don't think so, considering that the spectrum of amateur skills encompasses graduate engineers and scientists, as well as pure hobbyists. But what do you think? Should we find a place in QEX for engineering-level material such as this? Or is that kind of thing best left to *IEEE Transactions*?

Our New Internet Connection

ARRL HQ has just upgraded its

Internet connection. Previously, we connected to Performance Systems International (PSI), a provider of Internet services, via a 9600-bit/s dial-up line that gave us a dynamically assigned address. Since that address could be different each time we dropped the line and redialed, ARRL's presence on the Internet was one allowing only electronic mail. Our new connection is still via a dial-up line, but it's via a 14.4-kbit/s, V.42bis modem and to a dedicated port that gives us a fixed Internet address (38.1.129.1). In the coming weeks, we'll be settling in with this new connection and implementing limited FTP access—limited because at only 14.4-kbit/s, we can't support much in the way of 1-Mbyte file transfers! But we will support uploading of files and, of course, will continue to have a mail presence. We're excited about these improvements; they will let us communicate better with you.

This Month in QEX

A frequency counter is a useful tool, and even more so if you can read back the measurements with a computer, as with the "Personal Computer Frequency Counter," by John Nemeč, NS6Z.

In part 2 of 3, Ulrich L. Rohde, KA2WEU, continues his discussion of "All About Phase Noise in Oscillators" by describing the mathematical techniques used to model noise.

Darrel Emerson, AA7FV, has done some fascinating work using DSP to dig AO-13 ZRO test signals out of the noise. He describes his techniques in, "Digital Processing of Weak Signals Buried in Noise."

Finally, Zack Lau's (KH6CP/1) "RF" column presents a challenge for the reader. Zack has designed a 2-meter power amp—most of the way through. You have to provide the input and output matching networks. If you find a good solution, send it in to Zack. (If you're stuck, send Zack an sase and he'll show you his solutions.)—KE3Z, email: jbloom@arrl.org.

Personal Computer Frequency Counter

*A PC-based frequency counter provides
all kinds of measurement options.*

John Nemec, NS6Z

Accurate frequency measurement is an important test and alignment tool. Many amateurs use a low-cost frequency counter for this purpose, but stand-alone counters aren't always adequate; sometimes, you need to make multiple measurements. For example, to measure the frequency drift of your newly constructed VFO, you have to take a number of measurements at various times after turn-on. Or, for the determination of an IF pass-band frequency response, the frequency measurement must be taken many times as a signal is swept across the IF filters and the IF output level is measured. You then can make a frequency-response plot which graphically illustrates the pass-band characteristics. So, the frequency counter must be a part of a simple data-acquisition system where data can be automatically taken, then manipulated and plotted. To accomplish this, I constructed the high-performance, PC-compatible frequency counter described here.

Since I like to work with all types of amateur equipment, from HF radio

receivers to UHF transceivers, I designed a counter that provides:

- user-selectable frequency resolution of 1 Hz or 10 Hz,
- a frequency range of 0 to 1 GHz, and
- a PC add-in card interface.

Design of the Frequency Counter System

The hardware design is relatively straightforward. There are three major parts of the system: the time-base generator, which generates the counting gate; the frequency counting chain; and the PC interface, for counter control and data reading via software. I selected components with the maximum functionality, such as integrated counter chips. This reduces wiring and keeps cost low. Using field programmable gate arrays (FPGA) would have substantially reduced the number of components, but they require high-level-language design tools and programming equipment which are not available to most amateurs. Those who do have access to such resources could redesign most of the system into one or two FPGAs.

Software controls most aspects of the measurement operation via registers on the counter card. A control register allows the counting chain to be

cleared, arms the gate circuit to initiate a single gate pulse, and allows reading of the status and count values.

Circuit Operation

The frequency counter is little more than a long counter chain which can be read, cleared and gated. The gate enables or disables the signal to be measured at the input to the counter chain. Operation starts with the counter cleared. The gate is opened for a specific time period which is accurately controlled, say one second. While the gate is open, the counter chain counts the cycles of the input signal. Then, after the gate closes, the counter chain is at a count value which is the number of cycles that occurred in the time interval during which the gate was open. The counters are then read by the software to obtain the count value. Dividing this number by the time that the gate is open gives the frequency. After the counters are read, they are cleared in preparation for another count. The entire measurement cycle is constantly repeated to give a real-time measurement of frequency.

The interface to the PC, shown in Fig 2, is via the ISA expansion bus, which is the standard set of slots on a PC. The I/O port address range of the

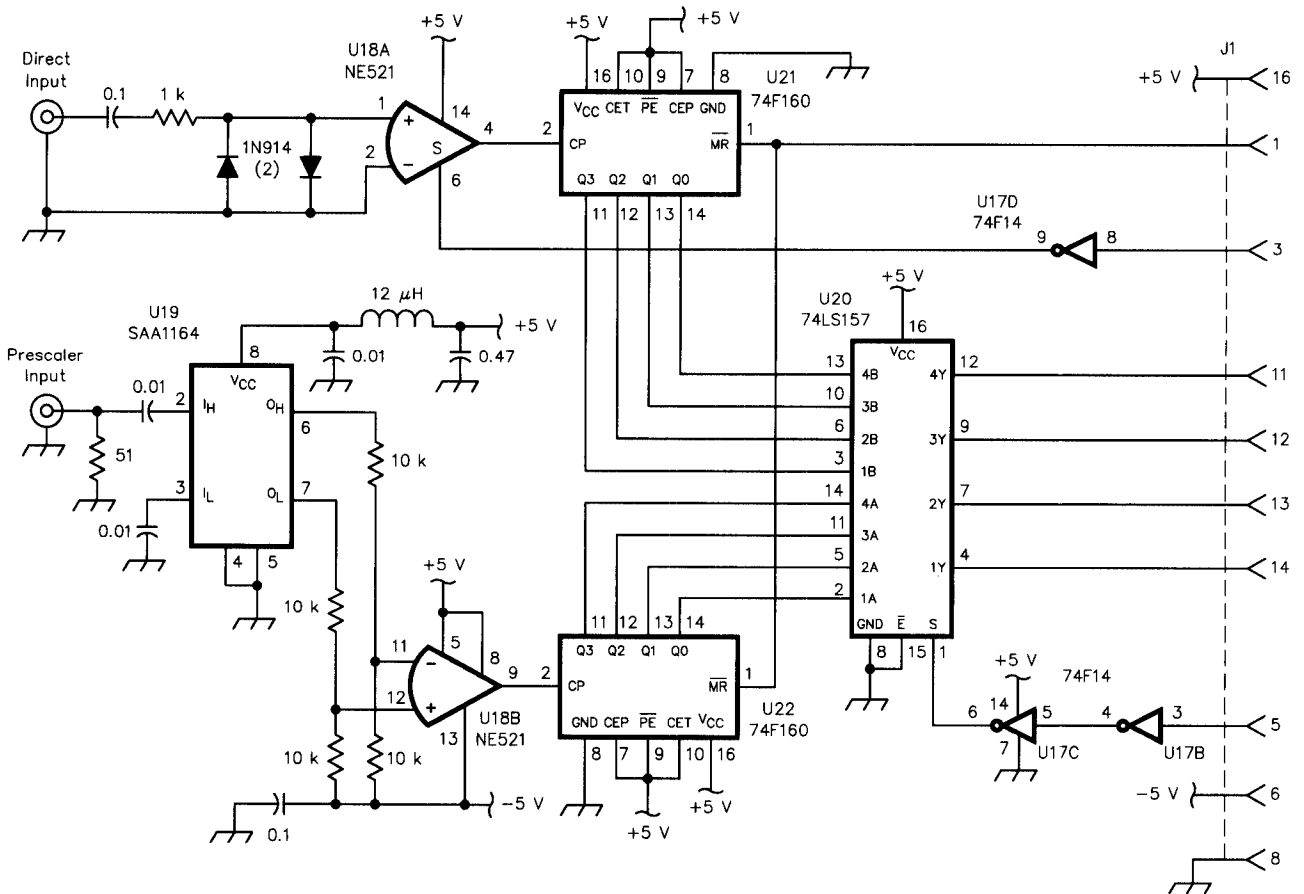


Fig 1—Schematic of the counter front-end daughter board. Use 0.1- μ F capacitors (not shown) from V_{cc} to ground at all IC sockets.

U17—74F14 hex Schottky inverter IC.
U18—NE521 dual high-speed comparator IC.

U19—SAA1164 1-GHz prescaler IC (see text for substitutes).

U20—74LS157 quad two-line-to-one-line mux IC.
U21,22—74F160 decade counter IC.

counter card is set by the decoding logic. U14 and U13 enable the card only when I/O addresses 300_{16} to 303_{16} are addressed. U10 and U15 generate strobe signals to enable reading and writing of the counter's registers. During reads of the card, U16 drives data from the card's internal data bus (IB0-7) onto the PC expansion bus. At all other times, U16 drives expansion-bus data onto the card's data lines.

The gate generator uses a 10-MHz crystal oscillator, U5, as its reference. This is divided down to 100 kHz by U3, then applied to a Philips HEF4750 CMOS frequency synthesizer, U2. Only the frequency-divider part of this IC is used in this circuit. It consists of a prescaler followed by a divide-by-N divider. The prescaler is configured to divide by either 10 or 100, as controlled on pin 23 of U2 by a bit of the control register (see Table 2). This bit effects 10- or 1-Hz resolution selection. The divide-by-N circuit is configured to divide by 1000. Thus U2 di-

vides by a total of either 10,000 or 100,000, as selected by the software. The resulting output of U2 (pin 26) is a 1-Hz or 10-Hz signal.

The counter is divided between the front-end section and a Philips HEF4534 CMOS counter, U4. U4 provides 5 decades of BCD counting, with the four bits of each decade appearing successively on the outputs of the IC. U8 provides the sixth decade, with the seventh, least-significant decade provided by either U21 or U22, in the "front end" circuit of Fig 1. One of the control-register bits (pin 6 of U12) provides a master counter-clear signal to each of the counter devices. This signal, along with the gate signal from U6, controls counter operation.

The front-end circuitry contains two counter chips, each of which is connected to its own input circuitry. U20, controlled by a bit of the control register, selects between the two counter chips. One of these chips, U21, counts the DIRECT input, which is conditioned

by U18A, a high-speed comparator. The PRESCALER input is applied to U19, a 1-GHz, ± 64 prescaler IC. Its output is converted to TTL levels by U18B and applied to U22 for counting.

Since the frequency counting chain

Fig 2—Schematic of the PC-based counter board. Use 0.1- μ F bypass capacitors (not shown) from V_{cc} to ground at all IC sockets.

U1—(not used)
U2—Philips HEF4750 frequency synthesizer IC.
U3—74LS390 decade counter IC.
U4—Philips HEF4534 5-decade frequency counter IC.
U5—10-MHz oscillator (see text).
U6—74LS74 dual D flip-flop IC.
U7—74LS04 hex inverter IC.
U8—74LS160 decade counter IC.
U9,11—74LS244 octal buffer IC.
U10—74LS32 quad OR gate IC.
U12—74LS374 octal D latch IC.
U13—74LS30 8-input NAND gate IC.
U14—74LS02 quad NOR gate IC.
U15—74LS139 dual 4-line decoder IC.
U16—74LS245 octal bus buffer IC.

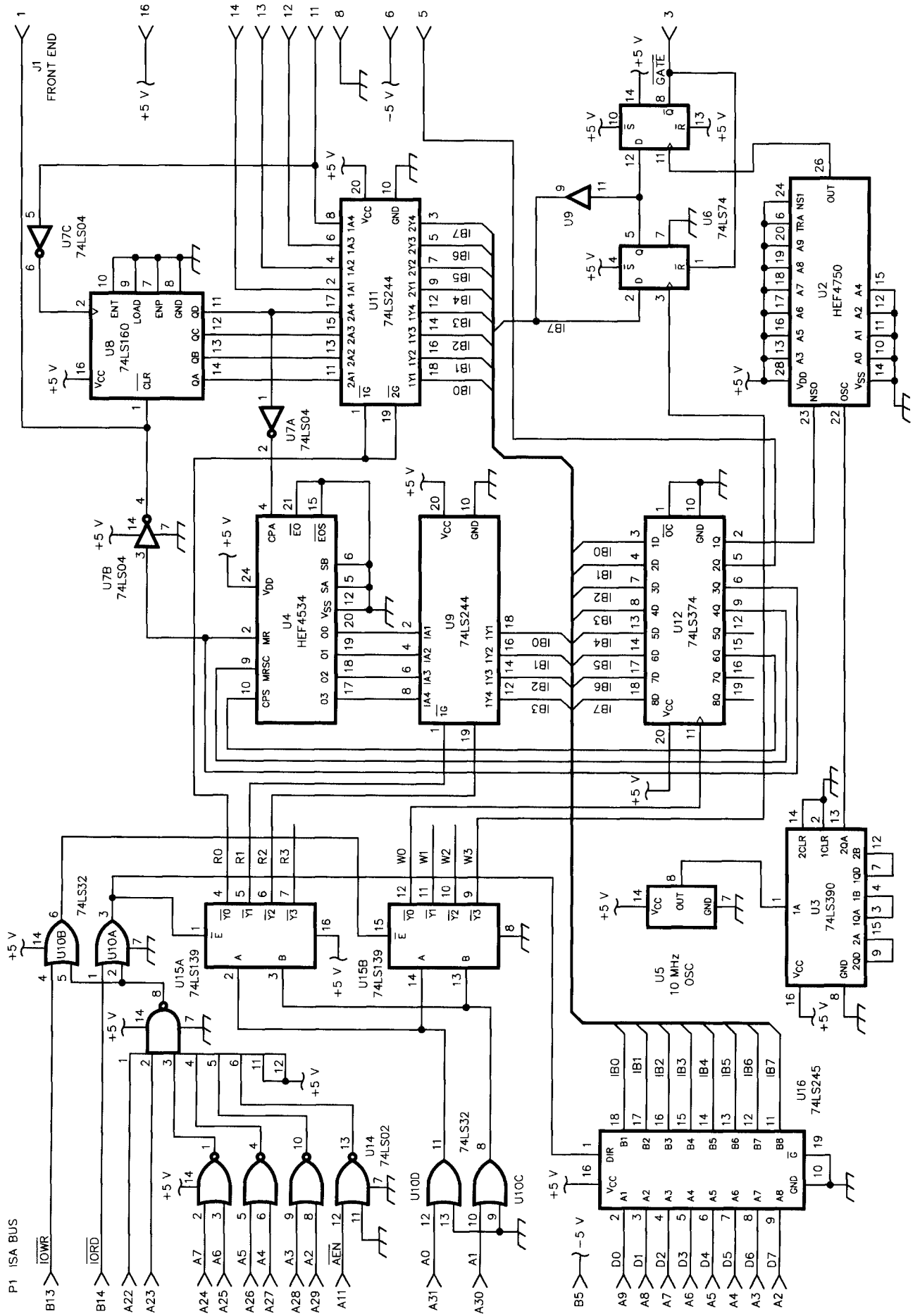


Table 1—Frequency Counter Registers

Address (hex)	R/W	Register
300	R	Least-significant decades
301	R	U4 data
302	R	Gate status (MSB)
303	R	(not used)
300	W	Control register (U12)
301	W	(not used)
302	W	(not used)
303	W	Gate arm

Table 2—Control Register Bits

Bit	Function
D0	0 = 1-second gate, 1 = 0.1-second gate
D1	0 = PRESCALER input, 1 = DIRECT input
D2	1 = clear counter chain
D3	U4 scan master reset
D4	(not used)
D5	U4 scan clock
D6	(not used)
D7	(not used)

is seven decades long, 1-Hz resolution (using a 1-second gate) with the DIRECT input can be achieved up to a frequency of 9.9 MHz. For higher frequencies, 10-Hz resolution (a 0.1-second gate) must be used, or the counter will overflow. (More resolution could be obtained by adding another counter to the frequency counting chain.) With the PRESCALER input selected, and with a 1-second gate, the resolution is 64 Hz. This resolution is usable up to just under 640 MHz (the 9.9-MHz limit discussed above times the prescaler ratio of 64). For frequencies above 640 MHz, a 0.1-second gate must be used, giving a resolution of 640 hertz.

PC Software

The program for running the frequency counter is written in Pascal and is shown in listing 1. It can be downloaded as file (QEXFQ194.ZIP) from the ARRL BBS (203-666-0578) or via the Internet from ftp.cs.buffalo.edu in the /pub/ham-radio directory.

The main program begins by setting the control byte to FF₁₆. This asserts the counter clear signal. The control byte is then changed to select the input source and gate time. After a delay, the control byte is modified again to remove the counter clear bit. Immediately after this, the gate is armed and the gate status register is monitored to verify that U6 has been set. Once verified, the gate status register is monitored, waiting for the end of the gate period. This sequence ensures that the gate has been opened and subsequently closed. Once this is completed, a valid frequency count is contained in the frequency counting chain.

The "getcount" procedure is called to read all of the counting chain contents. First, the two '160 decade counters—U21/22 and U8—are read and the results placed into two locations of the input-data array ("data"). Next, the 5

decades of data in U4 are read. Reading U4 is done by the "scanclk" procedure. This procedure toggles the HEF4534 scan clock input (pin 10 of U4) to advance the internal multiplexer through all of the five decades, placing the output of each one in turn on the device data output pins. (The scan clock is generated in software because the HEF4534 is too slow to respond directly to the PC I/O bus.) First the most significant digit is read, then the master reset for the HEF4534 scan (pin 9 of U4) is removed and the "scanclk" procedure is called to advance the HEF4534 output to the next digit. The process of toggling the scan clock and reading the data is repeated for the remaining decades. All seven decades of count result are now contained in the input-data array as BCD digits.

If the direct input has been selected, the BCD digits are used directly. If the prescaler is selected, the BCD digits in the array are combined into a single real (floating point) variable, "freq," which is then multiplied by 64 to account for the prescaler. Note that the software has been written so that the 0.1-second gate is automatically selected whenever the prescaler is selected.

At start-up the program looks to see if a key has been pressed on the keyboard. If not, the program bypasses the writing of a header on the console and only displays the newly acquired frequency measurement value. If a key has been pressed, the program reads the keystroke. If the key is F1 or F10, the program selects the 1-second gate or the prescaler input, respectively. If the key is "x" the program exits. Any other key is ignored. The program continuously loops, taking counter readings and displaying the results.

For those readers familiar with Pascal programming, the flow of the program should not appear difficult. Note the line {\$C-,U-} at the beginning

of the program listing. This may normally be omitted but is required for certain revisions of Borland's *Turbo Pascal* to allow the recognition of the Boolean function "KeyPressed."

Operation

Operation consists of connecting the signal to be measured and then running the control software program, FREQCNT. You can use the F1, F10, and "x" keys to control the counter.

The direct input consists of a series 1-k Ω resistor with two back-to-back diodes to ground. This represents a moderate impedance to sources. False readings can occur if the input signal amplitude is insufficient. In tests of the frequency counter, a 7-MHz signal from a grid dip meter caused a reading of 3.5 MHz at low amplitudes. Audio frequencies also are difficult to measure; the rise times of audio signals are so slow that the high-speed comparator responds to noise near the zero crossing point. This causes a higher reading than the frequency of the signal present. I made no attempt to correct for this in the design, since my intended application is RF work. There are several possible ways to condition audio frequency signals for measurement, including adding hysteresis, or by using a low performance comparator. Note, too, that the direct input may always display at least one count, even though no signal is present. This is due to the offset in the NE521 comparator. The polarity of this offset may be such that the gate signal is present at the comparator output. This places a 1 in the least significant counter. If this is bothersome, the one may be subtracted from the result in software, or a small amount of bias may be injected into the comparator input to prevent the gate from passing through when no signal is present.

The 1-GHz prescaler input is terminated in 50 Ω and connected to the SAA1164 through a capacitor, per the

manufacturer's recommendations. The guaranteed operating range for this device is approximately 70 MHz to 1 GHz, with an input voltage between 10-mV rms and 200-mV rms. The word approximately is used here since the operation is not guaranteed at low amplitudes at the low- and high-frequency extremes. For details, refer to the manufacturer's data sheet. The SAA1164 oscillates when no input signal is applied. Therefore, a frequency indication will be obtained in the prescaler mode with no input applied. This frequency is usually in the 700-MHz to 900-MHz range. Since the input to the prescaler is not protected, care should be taken so that the device is not permanently damaged by excessive input voltages. Attenuators should be used when large amplitude signals are to be measured. Other prescaler chips that are pin-compatible with the SAA1194 may be used, although I haven't tried them myself. These include the Motorola MC12073 and the Plessey SP4632.

Construction and Checkout

The high-frequency circuitry of Fig 1 is built on a small daughter board. This board is a double-sided board consisting of a V_{cc} plane on one side and a ground plane on the other side. Isolated plated-through holes provide device mounting. Other holes provide connections for V_{cc} and ground and for 0.1- μ F bypass capacitors at each device socket. The -5-V supply is connected as an individual wire with appropriate bypass to ground at both the SAA1164 and NE521 sockets. Follow high-frequency construction techniques. Keep leads short and use point-to-point wiring (no wire-wrap). This daughter board is mounted to the main PC plug-in board with screws. The main board can be constructed using normal wire wrap techniques. There is nothing critical about this circuitry. The daughter board is connected to the main board through a ribbon cable mated to two connectors, one on each board.

Initial check-out can be performed with the board out of the PC, with +5 and -5 volt supplies applied. In this way, simple shorts can be detected without endangering the PC. Examine pin 26 of the HEF4750 for the gate signal with a VTVM or logic probe. If no signal is present, use a logic probe or oscilloscope to trace the signal from the 10-MHz oscillator through the HEF4750.

Install the board in the PC for the

remaining checkout. Again using a logic probe, check the outputs of U15 and the direction output of U10, pin 3. A simple BASIC or Pascal program allows reading or writing the addresses of Table 2. (Or use DEBUG.)

Next, various values should be written to the control register, U12. All zeros with a walking 1 should be used to check each bit's appearance at the correct output at U12 and at the correct destination in the rest of the circuit. With this completed, all that remains is to check out the frequency counting chain. Using a clip lead, connect the PC I/O channel oscillator source (pin B30 of the edge connector) to the DIRECT input of the frequency counter card. Invoke the FREQCNT program to measure the frequency. For an ISA bus interface, this should be 14,318.18 kHz. If nothing appears, the counter chain may be nonfunctional. If a very different number appears, it is possible that the read circuitry is miswired.

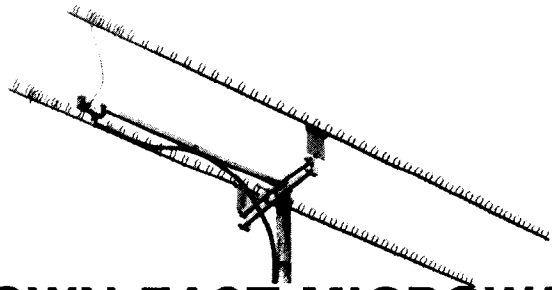
Applications and Additions

For greater accuracy, the user may wish to replace U5 with a tempera-

ture-compensated crystal oscillator, an oven-controlled crystal oscillator, or some external standard. If U5 is a standard crystal oscillator, I recommend that you check its accuracy by measuring a signal of known frequency. If the measurement is inaccurate, U5 can be replaced, or you can add an adjustment in software to scale the measurement. This should be checked periodically to adjust for crystal aging.

The control register, U12, contains unused outputs which could be tied to the set and reset inputs of U6 (pins 10 and 13). This would allow direct control of the gate so that the counter could be used as an event counter.

The software can be modified for additional features, too. For example, the inverse of the frequency—the period—can be displayed. The frequency counter can also be made part of a data acquisition system. For this purpose, the program can be modified to be a procedure called by a supervisory program. The measured frequency data can then be combined with other data to be analyzed or plotted. □□



DOWN EAST MICROWAVE
Amateur Microwave Antennas and Equipment

902, 1269, 1296, 2304, TROPO, EME, WEAK SIGNAL,
 2320, 2400, 3456 MHz OSCAR MODE L, MODES,
 ATV, REPEATERS

LOOP YAGIS, POWER DIVIDERS, COMPLETE ARRAYS
 KIT FORM OR ASSEMBLED AND TESTED
 SOLID STATE LINEAR AMPLIFIERS FOR 902 & 1296 MHz

Write for Free Catalog to:
DOWN EAST MICROWAVE
 Bill Olson W3HQT, Box 2310 RR1
 Troy, ME 04987 (207) 948-3741




All About Phase Noise In Oscillators

Part II—How oscillator phase noise is predicted

by Ulrich L. Rohde, KA2WEU

Calculation of Oscillator Noise

Linear Model

We will assume that the oscillator is composed of a linear amplifier with gain A and a high- Q resonant circuit, as illustrated in block diagram form in Fig 3b.¹ The gain of the resonant circuit has been normalized to unity at the resonant frequency f_o . The amplifier gain must be unity or greater in order for the circuit to oscillate. Let S represent the amplifier noise referred to the amplifier input. The white noise, N , per unit bandwidth at the amplifier input is given by

$$N = N_t + N_a = FkT \quad \text{Eq 19}$$

where N_t is the thermal noise, N_a is the noise contributed by the amplifier, and F is the amplifier noise factor. Therefore, the ratio of noise power per unit bandwidth to signal power, P_s , is FkT/P_s , which is a component of S_θ . In addition, amplifiers generate an additional *flicker*, or $1/f$ phase noise, about the carrier frequency due to carrier density fluctuations in the base resistance. A plot of S , shown in Fig 3c, demonstrates that for frequencies near the carrier, S_θ has a $1/f$ spectrum. At high frequencies the spectrum is

flat and equal to FkT/P_s , the thermal noise floor. The frequency, f_c , below which the spectrum has a $1/f$ shape depends on the characteristics of the individual amplifiers. For the circuit of Fig 3b with positive feedback and $A=1$, the closed-loop steady-state transfer function between the amplifier output and the amplifier input is given by

$$B(j\omega) = \frac{1}{1 - H(j\omega)} \quad \text{Eq 20}$$

where

$$H(j\omega) = \frac{1}{1 + jQ\left(\frac{\omega}{\omega_o} - \frac{\omega_o}{\omega}\right)} \quad \text{Eq 21}$$

Since $H(j\omega)$ is a high- Q filter, and we are interested in describing the noise power distribution about the center frequency, ω_o , $H(j\omega)$ can be replaced by its low-pass equivalent,

$$H_L(j\omega) = \frac{1}{1 + j\omega/\omega_L} \quad \text{Eq 22}$$

where

$$\omega_L = \frac{\omega_o}{2Q} \quad \text{Eq 23}$$

is the low-pass equivalent bandwidth. The noise spectral density, $S_o(\omega)$, at the output of a filter with a transfer function $G(j\omega)$, in terms of the spectral density of the input noise, $S_i(\omega)$, is given by

$$S_o(\omega) = S_i(\omega)|G(j\omega)|^2 \quad \text{Eq 24}$$

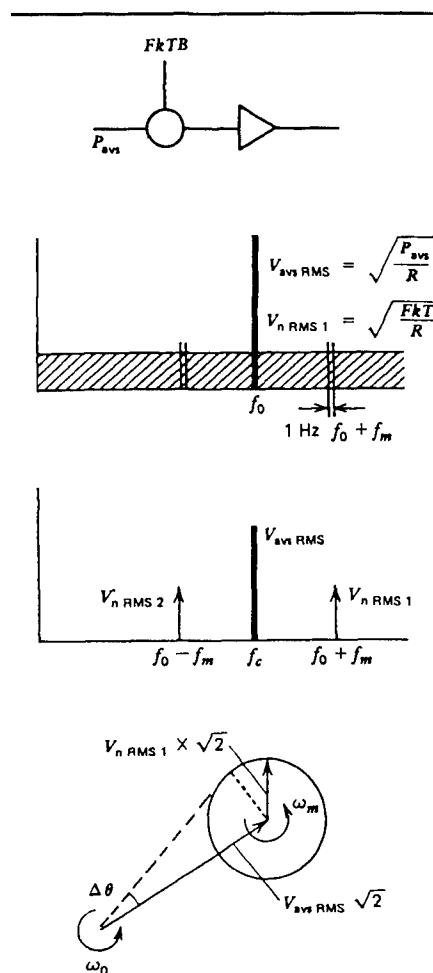


Fig 3a—Modulation medium that adds phase noise to carrier.

¹Notes appear on page 16.

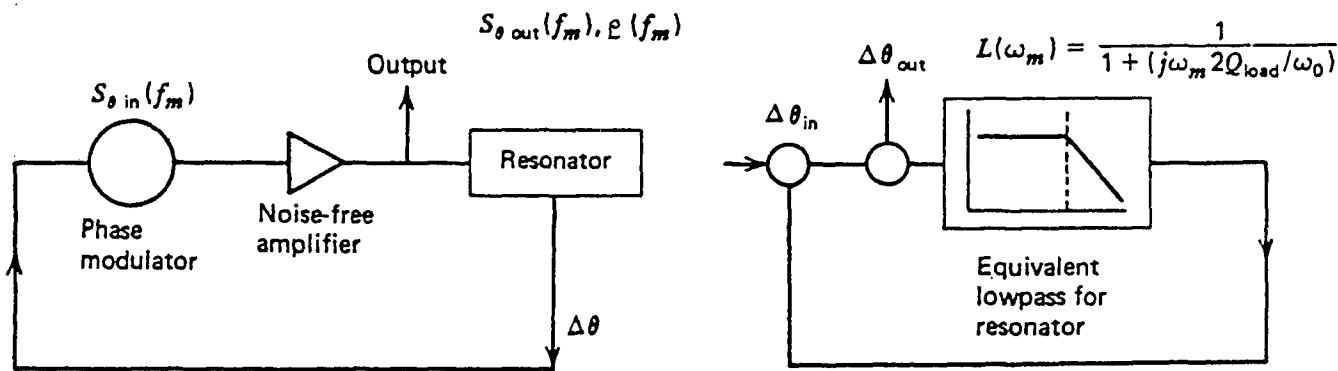


Fig 3b—Block diagram of the feedback model of an oscillator consisting of a phase modulator, noise-free amplifier and resonator.

so, the equivalent phase noise of the closed-loop system is

$$\begin{aligned}
 S_o &= S_\theta \frac{1}{|1 - H(\omega)|^2} \\
 &= \frac{S_\theta}{\left|1 - \frac{1}{1 + j\omega/\omega_L}\right| \left|1 - \frac{1}{1 - j\omega/\omega_L}\right|} \\
 &= \frac{S_\theta (1 + \omega^2/\omega_L^2)}{\omega^2/\omega_L^2} \\
 &= S_\theta \left(1 + \frac{\omega_L^2}{\omega^2}\right)
 \end{aligned}
 \tag{Eq 25}$$

which can be written using Eqs 5, 19 and 23 as,

$$S_o(\omega) = \frac{FkT}{P} \left(1 + \frac{\omega_o^2}{4Q^2\omega^2}\right)
 \tag{Eq 26}$$

which is the expression proposed by Leeson for describing the noise at the output of an oscillator.

As mentioned in Part 1, there are various types of noise, and so far Leeson's model does not contain an allowance for the flicker noise. We will, therefore, modify our equation into

$$L(f_m) = \frac{1}{2} \left[1 + \frac{1}{\omega_m^2} \left(\frac{\omega_o}{2Q_{load}}\right)^2\right] \frac{FkT}{P_{sav}} \left(1 + \frac{f_c}{f_m}\right)
 \tag{Eq 27}$$

This equation describes the phase noise at the output of the amplifier of the oscillator.

Fig 4 shows the difference in oscillator noise depending on the Q of the resistor. In accordance with Note 16, we will expand Leeson's equation further for an actual oscillator to show how the noise performance can be optimized. Loaded Q can be expressed as

$$\begin{aligned}
 Q_{load} &= \frac{\omega_o W_e}{P_{diss, total}} = \frac{\omega_o W_e}{P_{in} + P_{res} + P_{sig}} \\
 &= \frac{\text{reactive power}}{\text{total dissipated power}}
 \end{aligned}
 \tag{Eq 28}$$

where W_e is the reactive energy stored in L and C ,

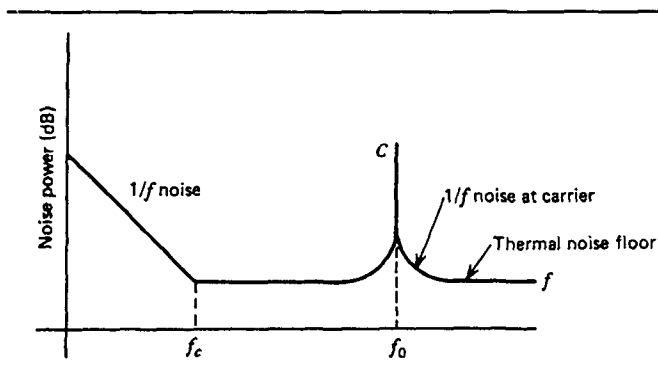


Fig 3c—Noise power versus frequency of a transistor amplifier with an input signal applied.

$$\begin{aligned}
 W_e &= \frac{1}{2} CV^2 & P_{res} &= \frac{\omega_o W_e}{Q_{unl}} & \tag{Eq 29} \\
 L(f_m) &= \frac{1}{2} \left[1 + \frac{\omega_o^2}{4\omega_m^2} \left(\frac{P_{in}}{\omega_o W_e} + \frac{1}{Q_{unl}} + \frac{P_{sig}}{\omega_o W_e}\right)^2\right] \left[\left(1 + \frac{\omega_c}{\omega_m}\right) \frac{FkT_o}{P_{sav}}\right] \\
 &\quad \text{input power over reactive power} & \text{resonator } Q & \text{ flicker effect} & \text{phase perturbation} \\
 &\quad \text{signal power over reactive power} & & &
 \end{aligned}$$

This equation is extremely significant because it contains most of the causes of phase noise in oscillators. To minimize the phase noise, the following design rules apply:

1. Maximize the unloaded Q .
2. Maximize the reactive energy by means of a high RF voltage across the resonator, and obtain a low LC ratio. The limits are set by the breakdown voltages of the active devices and the tuning diodes, and by the requirement to avoid a forward-bias condition of the tuning diodes.
3. Avoid saturation at all cost, and try to have either limiting or AGC without degradation of Q . Isolate the tuned circuit from the limiter or AGC circuit. Use antiparallel tuning diode connections to avoid forward bias.
4. Choose an active device with the lowest available noise

figure. Currently, the best bipolar transistor is the Siemens BFQ81, and the lowest-noise field-effect transistors are U310 and 2N5397, up to 500 MHz. The noise figure of interest is the noise figure obtained at the actual impedance at which the device is operated. When using field-effect transistors, it is preferable to deal with the equivalent noise voltage and noise currents rather than with the noise figure, since they are independent of source impedance. The noise figure improves as the ratio between source impedance and equivalent noise resistance increases. In addition, in a tuning circuit, the source impedance changes drastically as a function of the offset frequency, and this effect has to be considered.

5. Phase perturbation can be minimized by using high-impedance devices such as field-effect transistors, where the signal-to-noise ratio of the signal voltage relative to the equivalent noise voltage can be made very high. This also indicates that in the case of a limiter, the limited voltage should be as high as possible.

6. Choose an active device with low flicker noise. The effect of flicker noise can also be reduced by RF feedback. An unypassed emitter resistor of 10 to 30 ohms in a bipolar circuit can improve the flicker noise by as much as 40 dB. In a later example we will study such an oscillator.

The proper bias point of the active device is important, and precautions should be taken to prevent modulation of the input and output dynamic capacitance of the active device, which will cause amplitude-to-phase conversion and therefore introduce noise.

7. Finally, the energy should be coupled loosely from the resonator rather than from another portion of the active device, so that the resonator limits the bandwidth. A crystal oscillator using this principle is described later.

Equation 29 assumes that the phase perturbation and the flicker effect are the limiting factors, as practical use of such oscillators requires that an isolation amplifier be used.

In the event that the energy is taken directly from the resonator and the oscillator power can be increased above 0 dBm, the signal-to-noise ratio can be increased above the theoretical limit of -174 dB, due to the low-pass filter effect of the tuned resonator. But, this is mainly a theoretical assumption that does not represent the real world. In a real system, this noise perfor-

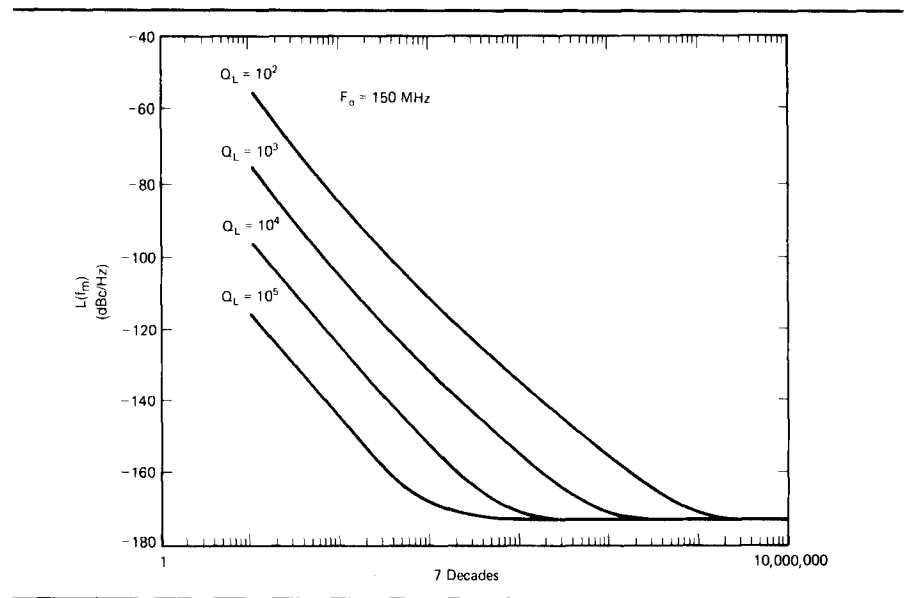


Fig 4—Noise sideband of an oscillator at 150 MHz as a function of the loaded Q of the resonator.

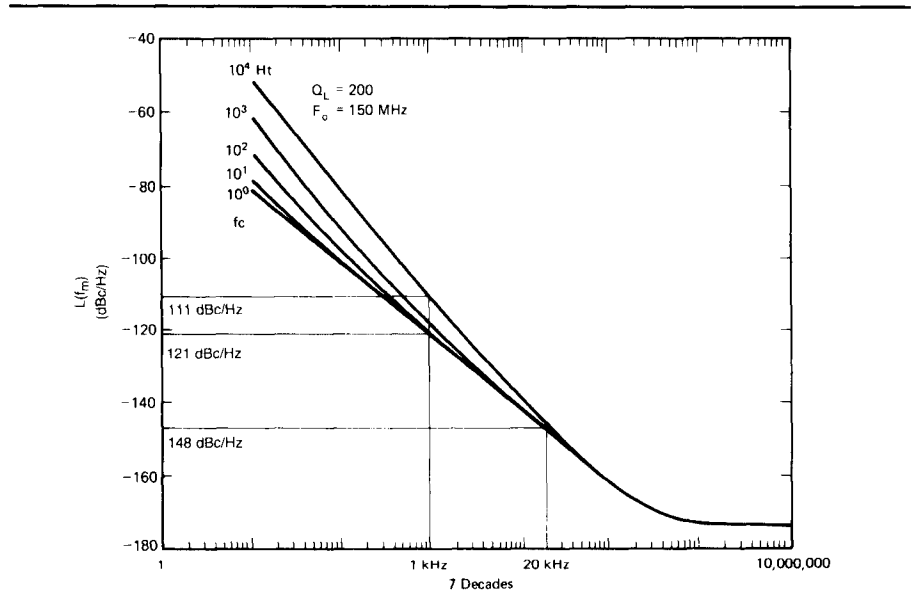


Fig 5—Noise sideband as a function of flicker frequency.

mance cannot be obtained. In an oscillator stage, even a total noise floor of -170 dB is rarely achieved.

What other influences do we have that cause the noise performance to degrade? So far, we have assumed that the Q of the tuned circuit is really determined only by the LC network and the loading effect of the transistor. In synthesizer applications, however, we find it necessary to add a tuning diode. The tuning diode has a substantially lower Q than that of a mica capacitor, or even a ceramic capacitor. As a result of this, the noise sidebands change as a function of the additional

loss. This is best expressed by adjusting the value for the loaded Q in Eq 27.

There seems to be no precise mathematical way of predetermining the noise influence of a tuning diode, but the following approximation of the Q that results from adding the tuning diode to the resonator seems to give proper results.

$$\frac{1}{Q_{Tload}} = \frac{1}{Q_{load}} + \frac{1}{Q_{diode}} \quad \text{Eq 30}$$

The loading effect of the tuning diode is due to losses, and these losses can be described by a resistor parallel to the tuned circuit. The tuning diode

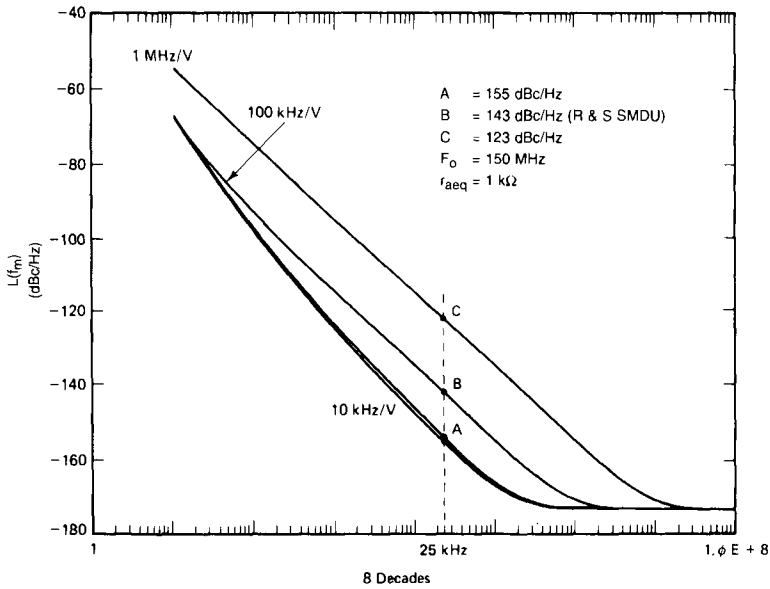


Fig 6—Noise sideband performance of an oscillator at 150 MHz, showing the influence of various tuning diodes and increased noise as a function of modulation sensitivity.

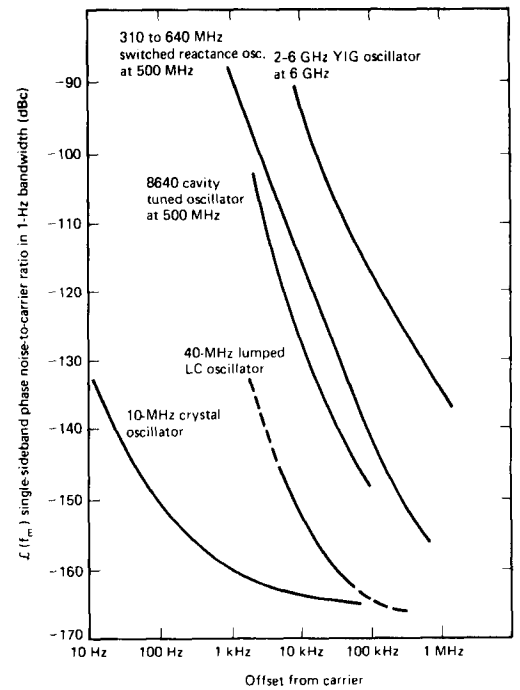


Fig 7—Comparison of noise sideband performance of a crystal oscillator, LC oscillator, cavity-tuned oscillator, switched reactance oscillator, and YIG oscillator.

is specified to have a cutoff frequency, f_{max} , which is determined from the loss resistor and the value of the junction capacitance as a function of voltage (ie, measured at 3 V). This means that the voltage determines the Q and, consequently, the noise bandwidth.

It is possible to define an equivalent noise R_{aeq} that, inserted in Nyquist's equation

$$V_n = \sqrt{4KT_o R \Delta f} \quad \text{Eq 31}$$

where $KT=4.2 \times 10^{-21}$ at about 300°K, R is the equivalent noise resistor, and f is the bandwidth, determines a noise voltage across the tuning diode. Practical values of R_{aeq} for carefully selected tuning diodes are in the vicinity of 1000 Ω to 50 k Ω .

For $R_{aeq}=10$ k:

$$V_n = \sqrt{4 \times 4.2 \times 10^{-21} \times 10,000}$$

The resulting noise voltage is

$$1.265 \times 10^{-8} \text{ V} \sqrt{\text{Hz}}.$$

This noise voltage, generated from the tuning diode, is now multiplied by the VCO gain, resulting in the rms frequency deviation

$$(\Delta f_{rms}) = K_o \times (1.256 \times 10^{-8} \text{ V}) \quad \text{Eq 32}$$

in a 1-Hz bandwidth

In order to translate this into the equivalent peak phase deviation,

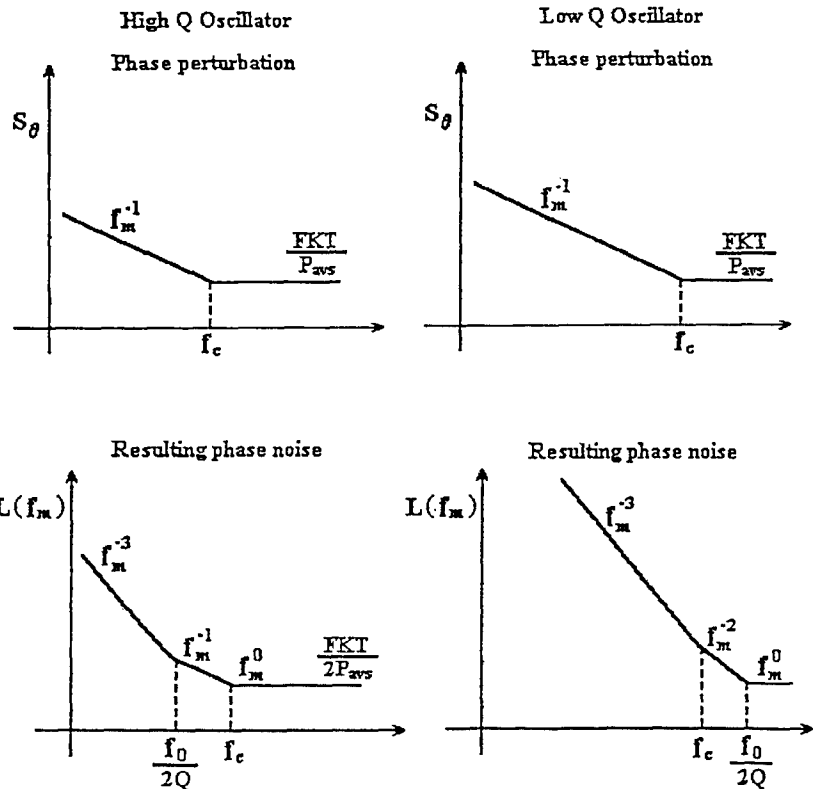


Fig 8—The spectral phase noise of the carrier-to-noise ratio versus frequency deviation from the carrier for low- and high-Q resonators.

$$\theta_d = \frac{K_o \sqrt{2}}{f_m} (1.265 \times 10^{-8} \text{ rad})$$

in 1-Hz bandwidth

or, for a typical oscillator gain of 100 kHz/V,

$$\theta_d = \frac{0.00179}{f_m} \text{ rad in 1-Hz bandwidth}$$

For $f_m = 25$ kHz (typical spacing for adjacent-channel measurements for FM mobile radios), $\theta_c = 7.17 \times 10^{-8}$. This can be converted now into the SSB signal-to-noise ratio

$$L(f_m) = 20 \log_{10} \frac{\theta_c}{2} \quad \text{Eq 33}$$

$$= -149 \text{ dBc/Hz}$$

This is the value typically achieved in the Rohde & Schwarz SMDU generator or with the Hewlett-Packard 8640 signal generator and is considered state-of-the-art for a free-running oscillator. It should be noted that these two signal generators use slightly different tuned circuits; the Rohde & Schwarz generator uses a helical resonator, whereas the Hewlett-Packard generator uses an electrically shortened quarter-wavelength cavity. Both generators are mechanically pretuned, and a tuning diode with a gain of about 100 kHz/V is used for frequency-modulation purposes or for the AFC input. It is apparent that, because of the nonlinearity of the tuning diode, the gain is different for low dc voltages than for high dc voltages. The impact of this is that the noise varies within the tuning range.

In many applications, VCOs are required to span large frequency ranges. This can be accomplished either solely with a tuning voltage, or by using switching diodes to select ranges via different tuning diodes or fixed reactances.

In low-energy-consuming circuits, the VCO frequently is divided into a coarse-tuning section and a fine-tuning section, both using tuning diodes. In the coarse-tuning range, this results in very high gains, such as 1 to 10 MHz/V, for the diodes. The noise contribution of those diodes is therefore very high and can hardly be compensated by the loop. For low-noise applications, which automatically mean higher power consumption, the use of switching diodes rather than high-gain tuning diodes is unavoidable.

Let us now examine some test results. If we go back to Eq 27 and Fig 4, they show the noise sideband perfor-

mance as a function of Q , where the top curve of Fig 4, with $Q_L = 100$, represents a somewhat poor oscillator, and the lower curve, with $Q_L = 100,000$, probably represents a crystal oscillator where the unloaded Q of the crystal was in the vicinity of 3×10^6 .

Fig 5 shows the influence of flicker noise. Corner frequencies of from 10 Hz to 10 kHz have been analyzed, and it becomes apparent that at around 1 kHz the influence of flicker noise is fairly dramatic, whereas its influence at 20 kHz from the carrier is not significant.

Finally, Fig 6 shows the influence of the tuning diodes on a high- Q oscillator. Curve A uses a lightly coupled tuning diode with a K_o of 10 kHz/V; the lower curve is the noise performance without any diode. As a result the two curves are almost identical, which can be seen from the somewhat smeared form of the graph. Curve B shows the influence of a tuning diode at 100 kHz/V and represents a value of -143 dBc/Hz, up from -155 dBc/Hz, already showing some deterioration. Curve C shows the noise if the tuning diode operates at a 1-MHz/V VCO gain, and the noise sideband at 25 kHz has now deteriorated to -123 dBc/Hz. These curves speak for themselves.

It is of interest to compare various oscillators. Fig 7 shows the noise performance of a 10-MHz crystal oscillator, 40-MHz LC oscillator, the HP 8640 cavity-tuned oscillator at 500 MHz, the 310- to 640-MHz switched reactance oscillator of the HP 8662 oscillator, and a 2- to 6-GHz YIG oscillator operating at 6 GHz.

The above theory of the linear approach has clearly indicated that the key factors for success in building a low-noise oscillator are:

1. Use a high- Q resonator, referring to the loaded Q .
2. Obtain the highest possible output from the oscillator while maintaining the smallest possible large-signal noise figure of the transistor.
3. Minimize the flicker noise and/or AM-to-PM conversion.

Fig 8 shows the carrier-to-phase-noise ratio versus the frequency offset from the carrier for low- and high- Q resonators. It is necessary to look at this plot to understand that the breakpoint for the corner frequency of the flicker frequency can move around as the Q changes. Remember also that Q is a function of loading the resonator with the transistor, and therefore the high-

est open-loop gain should be used.

Oscillators are frequently multiplied up to the actual desired output frequency. For microwave applications, frequencies between 2-10 GHz are often required. Fig 9 shows a phase noise comparison of YIG and varactor tuned oscillators normalized to a center frequency of 6 GHz. This represents the state-of-the-art in tunable oscillators; of course, crystal oscillators, oscillators with ceramic resonators and dielectric resonators have much better performance.

Nonlinear Model

The usual active device in an oscillator is either a bipolar transistor or a member of the FET family. Depending on the frequency range, FETs used for oscillators are either "N" junction FETs, MOS devices or GaAs FETs. In the case of bipolar transistors, the model of choice for nonlinear analysis is the Gummel-Poon bipolar transistor model, typically used in a modified version.

For the FET family, several nonlinear models are available. In the case of the GaAs FET, popular models are the Curtice-Edenberg, the Raytheon-Stutz, TOM, and Materka models. For MOS devices we choose a MOS level-3 Spice type model. These models are typically found in nonlinear circuit simulator programs such as Compact's *Microwave Harmonica*. These active devices are modeled by a variety of nonlinear elements such as diodes and voltage- and/or current-dependent capacitances which are the major form of nonlinearities. The device changes as a function of bias, and therefore the noise figure at each bias point is different. At high current levels, the noise, of course, will increase significantly. This requires the generation of a bias-dependent noise model which then is available for applications such as mixers and oscillators. A detailed introduction into this theory was presented in my previous paper.²

General Concept of Noise Contribution

In the evaluation of a noisy two-port network, it is important to know the amount of noise added to a signal passing through a network.

$$\frac{S_{in}}{N_{in}} \rightarrow \text{Network} \rightarrow \frac{S_{out}}{N_{out}} \quad \text{Eq 34}$$

An important parameter for expressing this characteristic is the noise factor (or noise figure).

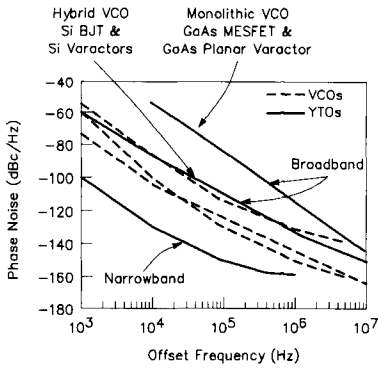


Fig 9—Phase noise comparison of YIG and varactor-tuned oscillators normalized to a center frequency of 6 GHz.

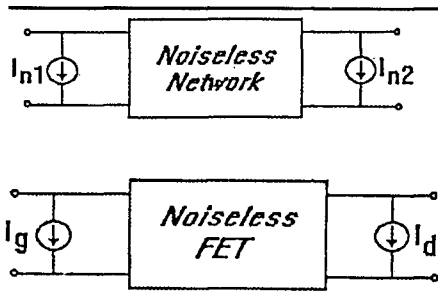


Fig 10—Noiseless FET with noise sources at the input and output.

$$\text{Noise Factor} = F = \frac{S_{in} / N_{in}}{S_{out} / N_{out}} \quad \text{Eq 35}$$

$$\text{Noise Figure} = \text{NF} = 10 \log (F)$$

The sources of the internal noise in a general circuit are:

- noise from linear elements
- thermal noise related to the admittance of the elements.

A noise network can be treated as a noiseless network with equivalent noise current source at each external port, such as is shown in Fig 10. The correlation of the noise current sources of a linear network is related to the Y matrix of this network:

$$C_n(\omega) = \frac{1}{\pi} K_B T \delta \omega [Y(\omega) + Y^*(\omega)] \quad \text{Eq 36}$$

The intrinsic noise sources of an active device (MESFET, BJT, ...) can be separated into a noiseless FET with noise sources at the input and the output as shown in Fig 11.

The intrinsic noise model can be expressed by the four measured parameters:

- F_{\min} - Minimum noise figure
- R_n - Equivalent normalized noise resistance = $r_n/50$

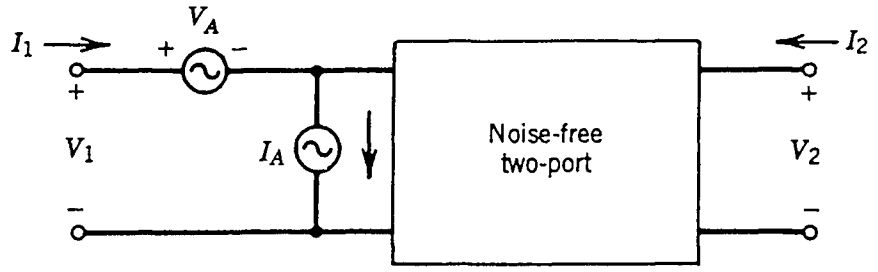


Fig 11—The intrinsic noise sources of an active device (MESFET, BJT,...) can be separated into a noiseless FET with noise sources at the input and output.

Noise power

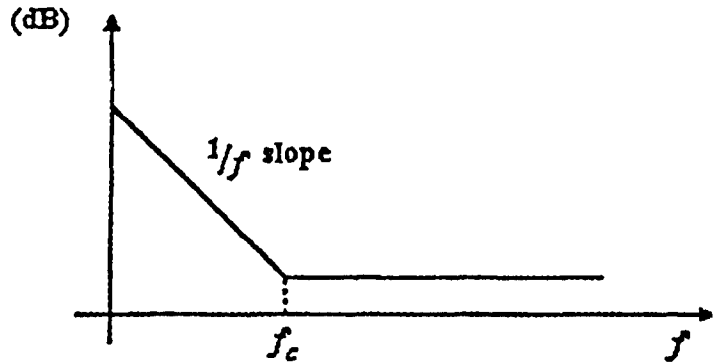


Fig 12—The major parameter used to describe the flicker noise is f_c —corner frequency.

M_{Go} - Magnitude of the optimal noise reflection coefficient

P_{Go} - Phase of the optimal noise reflection coefficient.

From these four parameters, the Van der Ziel noise model of the GaAs FET, as an example, can be derived as:

$$C_n(\omega) = \frac{2}{\pi} K_B T \delta \omega \begin{bmatrix} \frac{\omega^2 C_{gs}^2}{g_m} R & -j\omega C_{gs} \sqrt{PRC} \\ j\omega C_{gs} \sqrt{PRC} & g_m P \end{bmatrix} \quad \text{Eq 37}$$

This conversion for all active devices like FETs and bipolar transistors has been implemented in linear simulators like Compact's *Super-Compact* and *Microwave Harmonica*. In addition, we have to add the flicker noise contribution of an active device. Fig 12 shows the flicker noise as a function of frequency.

Large Signal Condition of the Active Device

We now look at the noise model of an

active device when pumped by an LO. The noise sources and equivalent-circuit model parameters are modulated by the LO. Fig 13 shows the variation of some parameters as a function of the LO power.

The noise correlation matrix of the device is now modulated by the LO. This means variation in the noise correlation component and nonlinear parameters such as:

$$R, P, C, g_m, C_{Gs}, \dots = F(V_{Gs}, V_{ds}) \quad \text{Eq 38}$$

In addition, for FETs, as an example, the flicker noise is modulated by the drain current using the following equation:

$$\langle |I_f|^2 \rangle = 2K_B T \delta \omega Q \frac{|I_D|^\beta}{f^a} \quad \text{Eq 39}$$

For the bipolar model we use a similar approach.

Calculation of the Phase Noise Spectrum of the Oscillator

For the calculation of the phase noise spectrum of the oscillator a nu-

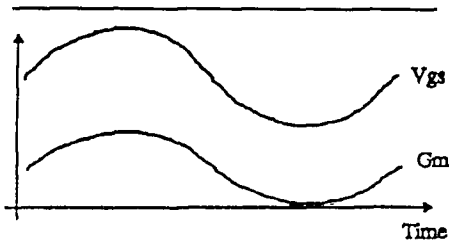


Fig 13—The voltages and currents of devices are determined by the harmonic balance calculations.

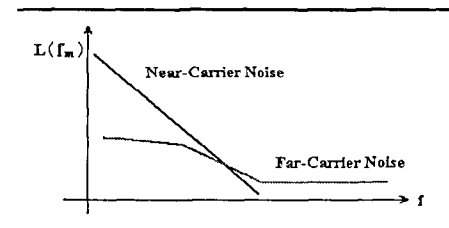


Fig 14—Oscillator noise consists of the near- and far-carrier noise.

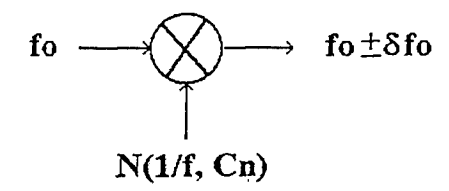


Fig 15—The mixing arrangement within the oscillator whereby the carrier frequency (f_o), assumed noiseless, gets modulated with the various noise sources.

merical approach is considered to provide nonlinear analysis. It can be shown that the phase noise is composed of two parts.

- The near-carrier noise consists of contributions from the perturbation of the oscillating frequency caused by the noise sources at each side band frequency. This part is the major noise source at near-carrier frequencies.

- The far-carrier noise consists of contributions from each sideband noise source through sideband-to-sideband transfer functions. This part is similar to a mixer noise calculation and is the major noise source at frequencies far from the carrier.

Fig 14 shows that the oscillator noise consists of the near- and far-carrier noise.

The Noise Figure of the Mixing Circuit

In order to calculate the noise figure,

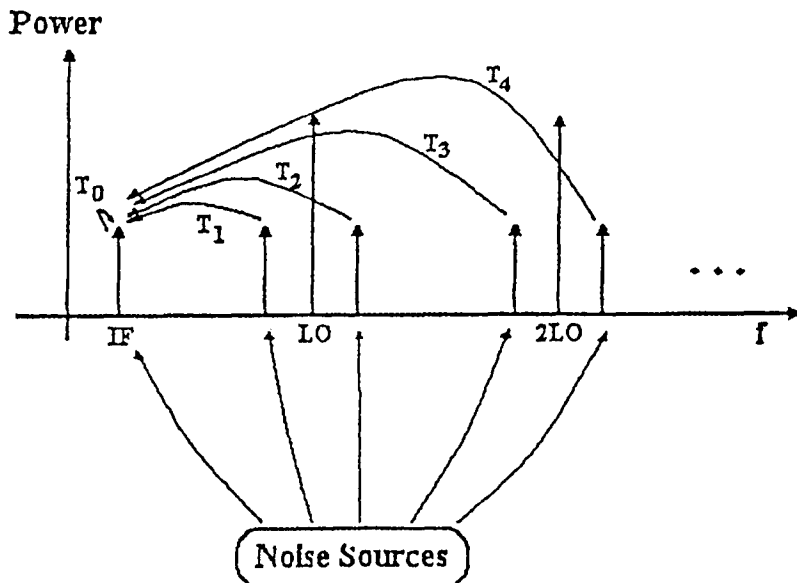


Fig 16—Summary of noise sources mixed to the IF. The noise at each sideband frequency contributes to the noise at the IF through frequency conversion.

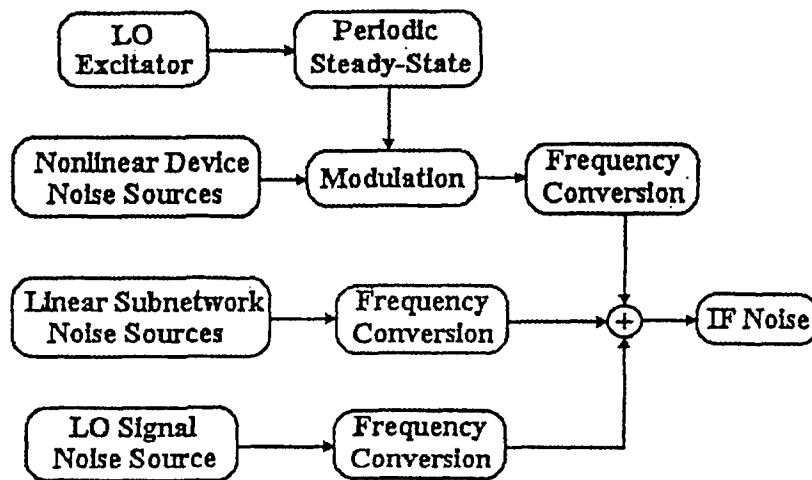


Fig 17—Summary of IF noise contributions.

we assume that the pumped active device acts like a mixer circuit; we need to calculate the total internal noise of the circuit at the "IF" frequency.

Noise Analysis Step 1

Using a nonlinear simulator, we perform a harmonic balance analysis to determine the steady state of the mixer. Fig 15 shows the mixing arrangement.

The harmonic balance calculation of the nonlinear simulator determines the Fourier coefficients of the voltages and currents of the circuit. Any re-

ceiver configuration (eg, LNA's, IF, AMP, etc) may be considered.

Noise Analysis Step 2

We next have to calculate the transfer functions of the sideband signals to the IF-band signal. Fig 16 shows a summary of noise sources mixed to the IF. The noise at each sideband frequency contributes to the noise at the IF through frequency conversion.

Fig 17 shows a summary of the IF noise contributions in a general nonlinear mixer circuit: note the large number of contributing elements

which make up the total noise at the output. The calculation of dN is performed by Eq 42 where the intermediate steps are given in Note 6. (See also Notes 3-14.)

$$\langle |\delta\Phi|^2(f_d) \rangle = \frac{\langle |V_l(f_d)|^2 \rangle + \langle |V_u(f_d)|^2 \rangle - 2 \operatorname{Re} \left\{ \langle V_l^*(f_d) V_u^*(f_d) \rangle \exp(2j\Phi_0) \right\}}{|V_0|^2} \quad \text{Eq 40}$$

$$\langle |\delta A|^2(f_d) \rangle = 2 \frac{\langle |V_l(f_d)|^2 \rangle + \langle |V_u(f_d)|^2 \rangle + 2 \operatorname{Re} \left\{ \langle V_l^*(f_d) V_u^*(f_d) \rangle \exp(2j\Phi_0) \right\}}{|V_0|^2} \quad \text{Eq 41}$$

$$\begin{aligned} dN(\omega_{IF}) &= R_{IF} \sum_p T_{0p} C_L(\omega_{IF} + p\omega_0) T_{0p}^* \\ &+ R_{IF} \sum_{p,q} T_{0p} \left[\sum_s H_{p-s} C_{dc}(\omega_{IF} + s\omega_0) H_{s-q} \right] T_{0q}^* \\ &+ R_{IF} \sum_{p,q} Y_p^s \left[\begin{array}{cc} \langle |V_u(\omega_{IF})|^2 \rangle & \langle V_u(\omega_{IF}) V_l^*(\omega_{IF}) \rangle \\ \langle V_u^*(\omega_{IF}) V_l(\omega_{IF}) \rangle & \langle |V_l(\omega_{IF})|^2 \rangle \end{array} \right] Y_q^{s*} \end{aligned} \quad \text{Eq 42}$$

In Eq 42, T_{0x} are the sideband-to-IF conversion matrices, H_x are the spectral modulation components of the device, the p, q, r , and s are sideband spectral indices, R_{IF} is the IF load, Y is a conversion admittance matrix between the LO noisy source and the IF load at the IF frequency, and ω_{IF} is a small frequency deviation in the neighborhood of the baseband frequency. The first term represents the noise contribution of the linear network, the second term is the noise contribution from the modulated non-linear devices, and the third term is the noise contribution of the noisy LO.

Calculation of the Total Carrier Phase Noise Spectrum

Under the assumption that the noise signals are small compared to the oscillator signal, the noise analysis is carried out as a perturbative analysis. The manner in which we determine the contributions is as follows:

- Far-carrier noise analysis (see mixer mode):

$$J_{BB} \delta X_B = -N_B(\omega) \quad \text{Eq 43}$$

- Near-carrier noise analysis:

$$J_{HH} \delta X_H = -N_H(\omega) \quad \text{Eq 44}$$

The near-carrier noise is the noise-induced jitter of the oscillatory steady state. The $\delta\omega$, one of the entries of δX_H , can be solved as

$$\delta\omega(\omega) = T_F [N_U(\omega) + N_L(\omega)] \quad \text{Eq 45}$$

and the resulting phase noise is

$$\begin{aligned} \langle |\delta\phi_k(\omega)|^2 \rangle &= (k^2 / \omega^2) \left[T_F \langle N_U(\omega) N_U(\omega)^+ \rangle T_F^+ \right. \\ &+ T_F \langle N_L(\omega) N_L^+(\omega) \rangle T_F^+ \\ &+ 2 \operatorname{Re} \left\{ T_F \langle N_U(\omega) N_L^+(\omega) \rangle T_F^+ \right\} \left. \right] \quad \text{Eq 46} \end{aligned}$$

In the linear case, the assumed simplification did not consider the AM/PM conversion and the change of the loaded Q as a function of the oscillator condition. The approach shown here is the exact solution for the calculation of the oscillator phase noise. Further details about the mathematical approaches are found in the literature cited.

Part 3 of this series will present some example circuits designed using these techniques.

Notes

- 1 Figs 1 and 2, Tables 1-3 and Eqs 1-18 appeared in Part 1, December 1993 QEX.
- 2 U.L. Rohde, C.R. Chang and J. Gerber, "Parameter Extraction for Large Signal Noise Models and Simulation of Noise in Large Signal Circuits Like Mixers and Oscillators," *Proceedings of the 23rd European Microwave Conference*, Madrid, Spain, Sept. 6-9, 1993.
- 3 C.R. Chang, "Mixer Noise Analysis Using the Enhanced Microwave Harmonica," *Compact Software Transmission Line News*, June, 1992, Vol 6, No. 2, pp 4-9.
- 4 T. Antognetti and G. Massobrio, *Semi-Conductor Device Modeling with SPICE*, McGraw-Hill, New York, NY, pg 91 (1988).
- 5 R.J. Hawkins, "Limitations of Nielsen's and Related Noise Equations Applied to Microwave Bipolar Transistors, and a New Expression for the Frequency and Current Dependent Noise Figure," *Solid State Electronics*, 20, pp 191-196 (1977).
- 6 Tzu-Hwa Hus, and Craig P. Snapp, "Low Noise Microwave Bipolar Transistor Sub-Half-Micrometer Emitter Width," *IEEE Transactions Electron Devices*, Vol ED-25, pp 723-730, June 1978.
- 7 R.A. Pucel and U. L. Rohde, "An Accurate Expression for the Noise Resistance R_n of a Bipolar Transistor for Use with the Hawkins Noise Model," *IEEE Microwave and Guided Wave Letters*, Vol 3, No. 2, February 1993, pp 35-37.
- 8 G. Vendelin, A. M. Pavio, and U. L. Rohde, *Microwave Circuit Design: Using Linear and Nonlinear Techniques*, John Wiley and Sons, New York (1990).
- 9 R.A. Pucel, W. Struble, Robert Hallgren, and U. L. Rohde, "A General Noise De-embedding Procedure for Packaged Two-Port Linear Active Devices," *IEEE Transactions on Microwave Theory and Techniques*, Vol 40, No. 11, Nov 1993, pp 2013-2024.
- 10 U.L. Rohde, "Improved Noise Modeling of GaAs FETS, Parts I and II: Using an Enhanced Equivalent Circuit Technique," *Microwave Journal*, November 1991, pp 87-101 and December 1991, pp 87-95, respectively.
- 11 V. Rizzoli, F. Mastri and C. Cecchetti, "Computer-Aided Noise Analysis of MESFET and HEMT Mixers," *IEEE Transactions on Microwave Theory and Techniques*, Vol MTT-37, pp 1401-1410, Sept 1989.
- 12 V. Rizzoli and A. Lippadri, "Computer-Aided Noise Analysis of Linear Multiport Networks of Arbitrary Topology," *IEEE Transactions on Microwave Theory and Techniques*, Vol MTT-33, Dec 1985, pp 1507-1512.
- 13 V. Rizzoli, F. Mastri, D. Masotti, "General-Purpose Noise Analysis of Forced Nonlinear Microwave Circuits," to be published in *Military Microwave 1992*.
- 14 V. Rizzoli, F. Mastri, and D. Masotti, "General-Purpose Noise Analysis of Forced Nonlinear Microwave Circuits," to be published in *Military Microwave 1992*.
- 15 V. Rizzoli, F. Mastri, and C. Cecchetti, "Computer-aided Noise Analysis of MESFET and HEMT Mixers," *IEEE Transactions on Microwave Theory Techniques*, Vol MTT-37, pp 1401-1410, Sept 1989.
- 16 Dieter Scherer, "Design Principles and Test Methods for Low Phase Noise RF and Microwave Sources," *RF and Microwave Measurement Symposium and Exhibition*, Hewlett-Packard. □□

Digital Processing of Weak Signals Buried in Noise

You think you can copy code in the noise? Read this!

Darrel Emerson, AA7FV/G3SYS

[Editor's note: This article first appeared as a paper in the *Proceedings of the AMSAT-NA Eleventh Space Symposium*.]

This article gives an example of digital signal processing (DSP) applied to the reception of very weak CW signals buried in noise. Using a very modest receiving antenna, the technique gave perfect reception of experimental CW transmissions from WA5ZIB via OSCAR 13 (AO-13) at ZRO level A, or 30 dB below the satellite beacon. Various DSP algorithms are used, and examples are shown of visualizing and searching for very weak signals buried in noise. The techniques are appropriate to low-power moonbounce (EME) communication, and have been used to search for weak leakage radiation from the defective OSCAR 13 Mode-JL transmitter.

Introduction

A few times a year, ZRO tests are conducted with AO-13 on downlink frequencies in the 70-cm (Mode JL)

and 2-m (Mode B) bands.¹ In these tests, CW blocks are sent with transmitted power decreasing in steps of 3 dB from a level (ZRO level 0) initially equal to the normal AO-13 beacon, down to a level 27 dB below the beacon (ZRO level 9). These tests present a challenge to improve receiving performance by trying to monitor the weakest possible signal level. Until 1992 only 2 stations, W7ID and DF7IT/DLØWH, had received the ZRO level-9 transmission perfectly at both downlink frequencies (see Note 1). As an additional experiment, in the spring of 1993 an even weaker signal (ZRO level A) was transmitted at a power level 30 dB below the normal AO-13 beacon.²

The receiving equipment I used for the ZRO tests was very modest; the antennas were circularly polarized crossed Yagis, a 10-element array on 2 m and an 8-element array for 70 cm. The receiver was a transverter feeding an HF rig with a 250-Hz bandwidth crystal filter and an optional active audio filter. On a good day, I could *sometimes* receive ZRO level 7. By ear I have never been able even to detect the presence of the level-9 signal, either on Mode B or Mode JL.

My home computer has a *Thunder Board* card from Media Vision, which is compatible with the well-known *Sound Blaster* board. My teenage children usually use the board for game sound effects, but it also can digitize 8-bit audio at sample rates between 4 kHz and 22 kHz. I decided to use the *Thunder Board* digitizer to record the ZRO signal from AO-13 through the audio output of my receiver, and to apply software processing to try to pull the weaker ZRO signals out of the noise. I have not yet tried to make the software run in real-time; this gives the great advantage that all programming can use a high-level language, with emphasis on making it easy to experiment with—and often reject—new data-processing algorithms. No thought was given to computing efficiency, which would have been a prime consideration for a real-time system.

The AO-13 ZRO tests are ideally suited to this DSP project. The total amount of information to be retrieved is very small—one new 5-digit number at each ZRO level. This means that many different algorithms can be tried without becoming swamped with problems of data storage or computer processing time. There is relatively little fading or interference on the satellite link, so the noise statistics should be very predictable, allowing

3555 E Thimble Peak
Tucson, AZ 85718
email: aa7fv@amsat.org (Internet)
74010,2230 (Compuserve)

¹Notes appear on page 24.

some straightforward statistical tests and analysis. The results were very successful: perfect copy was obtained even with the ZRO level-9 or level-A signal completely undetectable by ear. The sensitivity achievable with DSP techniques is quite remarkable.

Data Acquisition

The DSP technique described here has been applied very successfully to both Mode JL and Mode B ZRO transmissions from AO-13. The example here is from the Mode B ZRO transmission by Andy MacAllister, WA5ZIB, on 24 April 1993. The separate phases of this project are, in principle, quite simple and straightforward, but as always there are minor complications. The data acquisition should have been easy enough; plug the receiver audio output into the *Thunder Board* digitizer, tune the receiver to the right frequency in USB mode, point the antennas at AO-13, and wait for the ZRO tests to begin. However, the following details were found to be important:

1. *Interference.* At this level of sensitivity, interference from the computer was always a problem. I tried different computers, in different rooms of the house. The solution was to turn all computers off during the ZRO transmissions, and record the data on to an analog audio tape recorder. After the ZRO transmissions were over, the tape would be played back and digitized, using the standard .VOC file format to store the digitized data.

2. *Recorder quality.* The quality of analog audio recorders varies enormously. The critical parameters are a low frequency of dropouts, good tape speed stability on record and playback, and the absence of significant harmonics of the 60-Hz power frequency. I tested several different machines before choosing the most suitable.

3. *Automatic gain or level control (AGC or ALC).* Many analog audio recorders, and the *Thunder Board* digitizer, have an ALC loop to set the input level. This is very undesirable for recording the ZRO signal. I chose a recorder without ALC and carefully set the audio input level to the digitizer to be low enough to avoid ALC action on all but the strongest signals.

4. *Receiver filter bandwidth and frequency control.* In early tests I used maximum available selectivity in the receiver before digitization, including a 50-Hz bandwidth active audio filter. But the received frequency generally varies more than 50 Hz during a ZRO

test because of changing Doppler shift and other frequency drifts. Since steady drifts are easier to track in the data analysis than discrete frequency jumps, and because a digital analysis bandwidth of 8 Hz or less is used for the final analysis, Doppler tracking in discrete steps as large as 5 Hz would be unacceptable. It was found to be better to use a larger receiver bandwidth—250 Hz or more—and to rely entirely on digital processing to narrow down the selectivity and to track the frequency drifts.

6. *Digitization rate and disk space.* The lowest sample rate available on the *Thunder Board* is 4 kHz, which is much faster than the minimum sample rate strictly needed for a 250-Hz bandwidth. One full ZRO test can use 6 or 7 Mbytes of disk space for the .VOC file of raw data; the analysis may need much more space than this for intermediate stages of processed data. Computer disk management needs continuous attention.

Data Analysis

The various principles of digital signal processing are well known; a good summary and bibliography can be found in Note 3. The signals in this project are all weak, initially buried in noise. Processing is not attempted in real time, so programming convenience, rather than computer efficiency, is important. These factors guided the choice of algorithms. The software was written in FORTRAN specifically for this project, and consists of many stand-alone program modules that can be linked together at a higher level by procedure files. Where appropriate, existing subroutine libraries were used.^{4,5}

The DSP analysis tools used include:

- Fast Fourier Transform (FFT)
- Matched filters
- Tracking Finite Impulse Response (FIR) filter
- Convolution
- Cross- and auto-correlation
- Correlation coefficient and relative probability analysis
- Polynomial curve fitting, interpolation
- Data averaging to improve S/N ratio

The data display tools include:

- 2-D gray-scale graphical display of time & frequency intensities
- Line and X-Y plots of spectra and time sequences of data

The list of tools makes the analysis sound much more complicated than it really is. The principles are very simple. There are two distinct phases of the data analysis:

1. Finding the signal—the weaker ZRO levels cannot even be detected by ear, and

2. Retrieving the information from the modulation, once the basic signal has been identified.

The ZRO Signal

In finding and decoding the ZRO data, as much use as possible is made of prior information about the signal. The stronger ZRO signals (say ZRO level 0 to level 5) are heard easily and can be studied with very simple data processing. Both the Mode-B transmission from WA5ZIB and the Mode-JL signal from N5EM clearly use machine-generated CW. The precise speed and timing of the CW transmissions were derived from the stronger ZRO levels. Much of the later data processing uses this predictability of machine-sent CW to distinguish signal from noise in a way very similar to that described many years ago for the reception of coherent CW, but in this case with synchronization derived from known characteristics of the signal itself.⁶

Although the ZRO data are sent in CW at a nominal 10 WPM, the characteristics of the CW from WA5ZIB on Mode B are very different from those of N5EM on Mode JL. The WA5ZIB CW is at a strict 10 WPM in all respects, in timing of dots, dashes, intercharacter and interword spaces. The CW from N5EM was found to be sent in the Farnsworth manner; the individual characters were sent at 13 WPM, with longer intercharacter spaces to keep the average CW speed at 10 WPM. This is critical to the data analysis. There is an interesting implication for the relative limits of sensitivity; because the individual CW characters from N5EM are somewhat faster, the matched filter used to recover N5EM's signal needs to be wider, letting in more noise, with shorter averaging times possible for the post-detection signal. This gives about 1-dB S/N penalty to the ultimate sensitivity achievable on the N5EM signal, compared with the true 10 WPM data sent by WA5ZIB.

For each ZRO level, there is typically a short transmission of unmodulated carrier as WA5ZIB or N5EM adjust the transmitter power level, followed by three 5-figure groups identifying the ZRO level, then the

three 5-digit groups to be copied. For example, a level-9 transmission might consist of:

99999 99999 99999 12345 12345
12345

where "12345" represents the unknown 5-digit number group to be copied to prove reception at this level. If the "99999 99999 99999" sequence—or "AAAAA AAAAA AAAAA" for the level-A test—can somehow be detected in the noise, then the known timing of the machine-sent CW can be used to predict precisely when the first dot or dash of each "12345" or unknown sequence begins.

Identifying the Signal

Perhaps fortunately, it is much easier to detect the presence of a weak signal than to decode its modulation. Fig 1 shows an example test spectrum generated by digitizing the 983-Hz keyed audio tone output from an electronic keyer sending a repeating sequence of "1234567890" in CW at 10 WPM. The raw test data were subdivided into overlapping 2-second blocks, each containing 8192 data samples. A fast Fourier transform (FFT) was then made of each block, converting the raw numbers sampling the signal in time into a sequence of numbers describing the frequency spectrum of that block of data. Power spectra derived from many such 2-second blocks were averaged together to produce the average power spectrum, with a frequency resolution of about 0.5 Hz, shown in Fig 1. It shows that the highest energy density in this CW sequence is contained within less than 1 Hz of the central carrier. The sideband peaks at ± 4.2 Hz and ± 12.5 Hz result from regular sequences of dots (eg, a "5" in CW at 10 WPM resembles 5 cycles of square-wave signal at 4.17 Hz). These sidebands repeat at intervals of 8.33 Hz, gradually diminishing in amplitude away from the central carrier. The recognition of CW characters is only possible from the CW sidebands. However, for the first stage of analysis, only the detection of a signal—not interpretation of the modulation—is needed. The focus initially is on searching for the central spike of energy, allowing the use of a very narrow filter to improve the detection sensitivity.

Fig 2 shows a gray-scale representation of the changing frequency spectrum received from AO-13 during part of the ZRO level-9 transmission, and the entire ZRO level-A test transmitted by WA5ZIB on 24 April 1993. Each

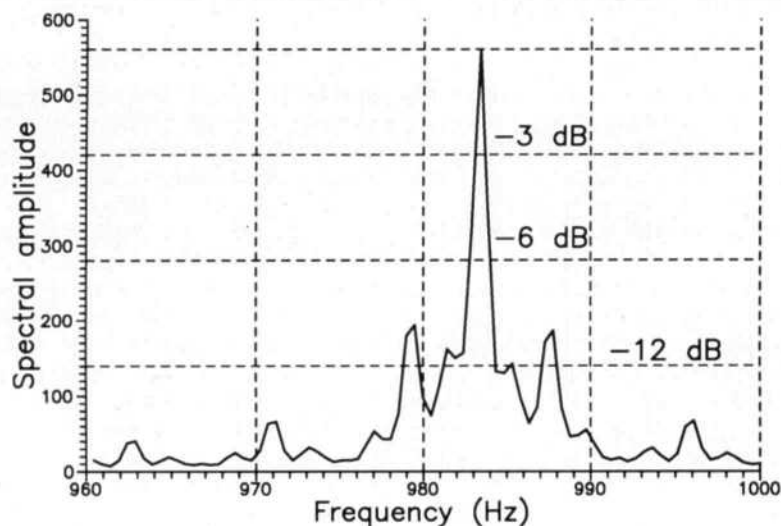


Fig 1—Average spectrum of a keyed 983-Hz tone from an electronic key sending a repeating sequence of "1234567890" in CW at 10 WPM. This shows that the highest energy density is within <1 Hz of the central carrier frequency.

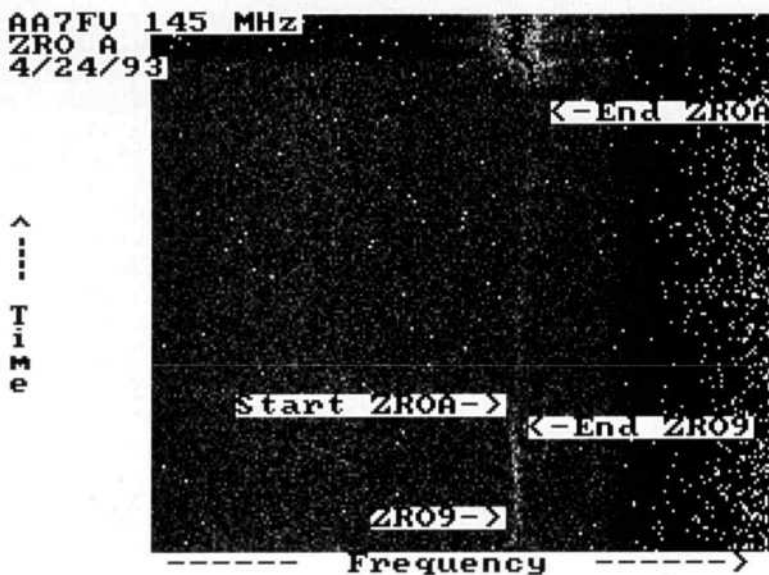


Fig 2—A 2-D gray-scale representation of power spectra against time. The horizontal axis is frequency and covers a frequency span of 390 Hz; the vertical axis is time, increasing from bottom to top, and covers 100 seconds of data. Each pixel corresponds to the intensity in 2 Hz of bandwidth averaged over 0.5 seconds of time, with higher intensities shown white. The end of the ZRO level-9 signal shows as the faint white vertical line in the lower part of the plot. The ZRO level-A signal is just visible as an extremely faint near-vertical line extending between the "Start ZROA" and "End ZROA" labels.

horizontal row of the plot represents a separate power spectrum; the spectral intensity is represented by varying shades of gray, with white indicating higher power. Each row is derived from a Fourier transform of 0.5 seconds of data, which yields a frequency resolution of 2 Hz. There are ~200

rows in this plot, covering 100 seconds of digitized data; time increases from bottom to top. A total range of 390 Hz is represented, with frequency increasing from left to right. Each pixel of the plot represents the average intensity in a 2-Hz band, averaged over 0.5 seconds of time. The purpose of the

display is to show the presence of any weak signal without attempting to decode the modulation.

The broad background of speckled dots in Fig 2, covering most of the plot, is due to receiver noise; the edge of the receiver's IF filter causes the gradual roll-off in noise intensity in the right of the plot. At the start of the data—at the bottom of the plot—the ZRO level-9 transmission is in progress and shows as the vertical white line. After about 20 seconds of data, the ZRO level-9 signal gives way to the level-A signal, which shows as a much fainter white line continuing upwards beyond the level-9 signal. This signal slopes slightly to the right, corresponding to a changing Doppler shift of the signal received from the satellite, combined with any other receiver or transmitter drifts. About 12 seconds before the end of the data represented here, near the top of the plot, the signal returns to higher power. After 2 or 3 seconds, WA5ZIB adjusted his transmitter to full power and began the "End of test" CW message; simultaneously, the frequency dropped lower by a few hertz. The CW modulation sidebands show for the final few seconds of data—the very top of Fig 2.

This type of representation of weak narrow-band signals buried in noise is very powerful. By ear, no trace whatsoever of the ZRO level-9 signal could be detected, yet it appears very clearly in the lower part of the gray-scale plot, with a clear detection of the even weaker level-A signal. This type of display has been used by astronomers engaged in the search for extra-terrestrial intelligence (SETI). The human eye is particularly good at discerning weak coherent patterns, such as faint lines, otherwise hidden in noise.

Apart from just detecting the weak ZRO level-A signal, Fig 2 also allows a determination of the rate of frequency drift of the received signal. The gradual shift to the right of the line showing the ZRO signal in Fig 2 suggests a frequency drift of about 15 Hz during the level-A transmission. Since the decoding of the CW modulation will use a matched filter of nominal bandwidth of 8 Hz, a correction has to be made for this drift. The frequency drift results from a combination of changing Doppler shift and any instabilities in the transmitter, satellite transponder, and receiver; a combined oscillator drift of less than one part in a hundred million is enough to be very noticeable, but is probably inevitable. Peaks of signal along the weak ZRO

level-A transmission shown in Fig 2 were picked out, and a simple 2nd or 3rd order polynomial was fitted to the points to give an empirical analytic expression for the instantaneous frequency at any moment during the ZRO level-A transmission. Later stages of signal analysis use this.

One last piece of information from Fig 2 concerns the short-term stability of the signal. The ZRO level-9 signal shows that there may be a frequency jitter of about 2 Hz in the received signal with a timescale of one or two seconds. Similar plots of the stronger ZRO level signals show the effect much more clearly. This fact alone shows that there would be little gain in going to even higher resolution, say to better than 2 Hz. Plots similar to Fig 2 but with 0.5-Hz frequency resolution were made, and these confirmed that there was no improvement in detection sensitivity. Any of the local oscillators in the Earth-satellite-Earth link could be responsible. The frequency jitter is also a phase jitter; an attempt to apply a phase-coherent detection algorithm was unsuccessful. If the RF phase of a given dot or dash element could be predicted from the average phase of the signal before and after that dot, taking into account the known slow but steady drift in frequency, then coherent demodulation could be used. In principle this could gain 3 dB in S/N ratio. It was found that the phase jumped randomly on a time comparable to the duration of a CW dot or dash, so the RF phase of any given CW dot could

not be predicted from the average phase of the neighboring signal. Thus nothing would be gained over normal incoherent (square-law) detection of the filtered signal.

Decoding the Signal

So far, the ZRO level-A signal has been identified, but no modulation information has been retrieved. To decode the CW modulation, a matched filter is required that allows the CW sidebands to pass, without admitting unnecessary noise. Fig 1 shows the typical spectrum to be expected from the CW signal. A digital matched filter was made based on the spectrum of a single dot element, widened a little to allow for the small but unpredictable frequency jitter found in the signal, and tapered a little to allow for the anticipated waveform shaping at the transmitter and to reduce the far-out frequency response. Fig 3 shows the response of the central 40 Hz of this filter to a steady 980-Hz tone. The first and successive sidebands of this matched filter coincide exactly with the narrower sidebands observed in the CW spectrum of Fig 1. In both signal (eg, Fig 1) and filter (Fig 3), there are minima in the response at $\pm 8.33, 16.67, 25.0 \dots$ Hz. The filter (voltage) passband shape is a slightly modified $\sin(x)/x$ function; the width between 3-dB points is 7.4 Hz, but the filter sidebands extend much further. The filter admits the same noise power as a perfectly rectangular filter width of 8.33 Hz. Elsewhere in this article it is simply referred to as an 8-Hz filter.

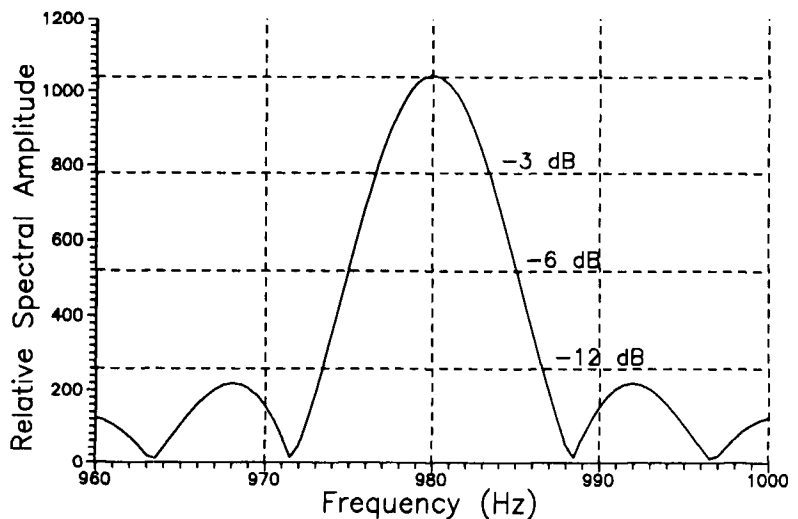


Fig 3—The central 40 Hz of the response of the DSP filter used to recover the CW modulation from the ZRO transmission. This filter was made to track the changing signal frequency.

The matched filter was implemented as an FIR filter, but one that tracks the signal in frequency. It was used to extract the ZRO level-A signal visible as the faint near-vertical track in Fig 2. The filter effectively averages the signal over the duration of one dot period (120 ms), but with some oversampling it was made to give a measure of the ZRO signal every 40 ms. The output, after demodulation with a perfect square-law detector, is plotted in Fig 4. This shows the end of the period of the ZRO level-9 signal, followed by the first few seconds of the ZRO level-A signal. The filter has tracked the slowly changing frequency of the signal seen in Fig 2, using a passband (Fig 3) that includes the important CW sidebands. Fig 4 shows the expected drop in average intensity from the level-9 down to the level-A signal, but the noise is still too high to permit discrimination of single dots or dashes, or even the gaps between individual CW characters.

To obtain an estimate of the real S/N ratio of the ZRO level-A signal, and to give confidence that the signal really is there, I made an average power spectrum. To do this, the same FIR 8-Hz filter was used to generate a complete power spectrum of the signal every 40 milliseconds, tracking the frequency drift. (The filter could equally, and more efficiently, have been implemented using multiple FFTs.) These 1000 or more spectra were averaged to give the mean power spectrum of the ZRO level-A signal, shown in Fig 5. This very clearly shows the weak ZRO signal at 835 Hz sitting on a general plateau of receiver background noise. A total frequency span of nearly 200 Hz is shown, but above about 890 Hz the response rolls off due to the passband of the receiver IF filter. In the 8-Hz passband, the mean power of the ZRO level-A signal is only 2.2 dB above the background noise floor.

Some much more sophisticated technique than trying to identify individual dots and dashes is needed to decode data such as that shown in Fig 4. One possible algorithm uses cross-correlations of the noisy data with known patterns; the more complex and the longer the known pattern, the more likely it is to find a good match to an identical pattern buried in noise within the data. The cross-correlation, or convolution, of a data array $x(j)$ with another array $y(i)$, where i ranges from $-n/2$ to $+n/2$, may be defined by:

$$z(j) = \sum_{i=-n/2}^{i=+n/2} x(i+j) \cdot y(i)$$

That is, the two arrays are put side by side, and the adjacent cross-products are summed. This gives one point of the cross-correlation function. One of the arrays is then displaced by one element, and the new adjacent cross-products are summed, to give the next point of the cross-correlation. This process is repeated until the entire cross-correlation pattern has been computed. At any point (j) in this process where the two arrays match well, most of the cross-products $[x(i+j) \cdot y(i)]$

will be positive, increasing the resultant summation, giving a high value for the correlation function at that point. If the two arrays are uncorrelated, some of the cross-products will be positive, but some negative; on average, they will sum to something close to zero, giving a very low value for the correlation function at that point.

As an example, Fig 6 shows a convolution of the CW pattern for "AAAAA AAAAA" with an identical model pattern without noise. There are three strong peaks, corresponding to where the patterns match, or correlate, best. The main peak, labeled (1),

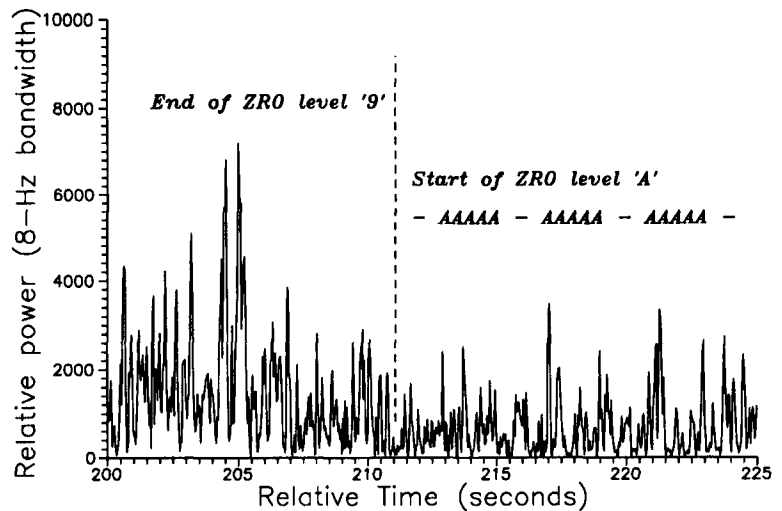


Fig 4—The detected output power, using the 8-Hz bandwidth matched filter, of the end of ZRO level 9, followed by the start of ZRO level A. The signal is too noisy to be able to discern individual dots and dashes.

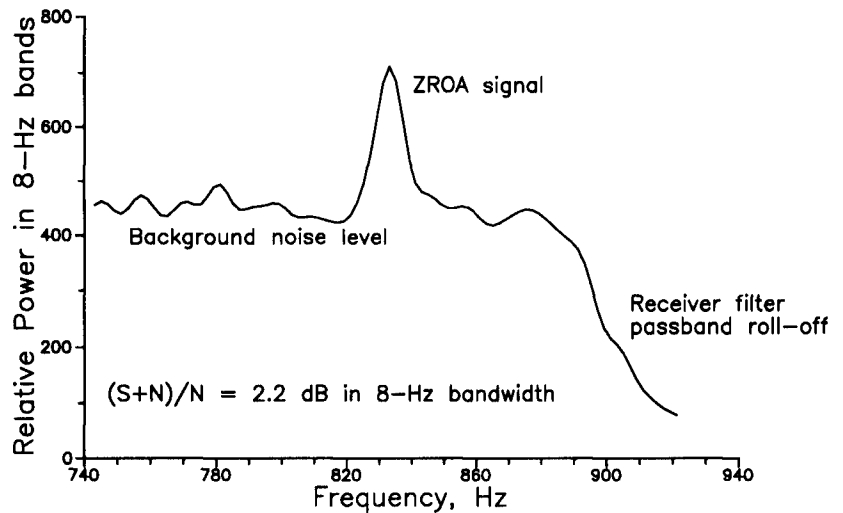


Fig 5—An average power spectrum covering the period of the ZRO level-A transmission made using a tracking FIR filter to allow for the drift in frequency.

corresponds to perfect alignment of the two patterns. The subsidiary peaks, marked (2) and (3) show somewhat weaker correlation; they correspond to where one pattern is shifted in time by exactly one whole 5-letter group. Two of the three 5-letter groups still match perfectly.

Fig 7 shows a convolution of the same CW pattern for "AAAAA AAAAA AAAAA" with the ZRO level-A data of Fig 4. The result (a cross-correlation function) shows three main peaks of correlation, labelled (1), (2) and (3), corresponding—albeit with added noise—exactly to the labelled peaks of the model data shown in Fig 6. The final confirmation comes from measuring the separation in time of these peaks; this agrees, to within a few milliseconds, with that predicted from the known timing of WA5ZIB's CW, derived earlier from the stronger ZRO levels. The position of the expected "AAAAA AAAAA AAAAA" sequence in the ZRO level-A data has been found without having to identify individual dots and dashes at all. This time information is critical; we can now calculate the exact start of the first dot or dash of the unknown ZRO level-A data using the identification of the expected "AAAAA ..." sequence as a synchronization pulse.

Initially, using this precise timing information, an attempt was made to decode the ZRO level-A data, letter by letter, as would have been done with true coherent CW. Although this worked well for ZRO level 9, the weaker level-A data needed a more powerful algorithm. A brute force approach was adopted, making trial cross-correlations of the data with all possible combinations of a 5-digit sequence. There are only 100,000 possible combinations! Starting with the CW pattern for "00000 00000 00000," then "00001 00001 00001" and working through to the final "99999 99999 99999" all possible combinations were tried to see which gave the best match, or relative degree of correlation, at the required instant. This requires very precise knowledge of and stability in the sending CW timing. When several possible, or most likely answers had been identified from this correlation technique, a convolution of the best candidate answer with the raw data was made to produce another plot with peaks equivalent to (1), (2) and (3) shown earlier in Figs 6 and 7. In this case, it was found that the separations of these peaks were not quite identical, but implied a drift in apparent CW

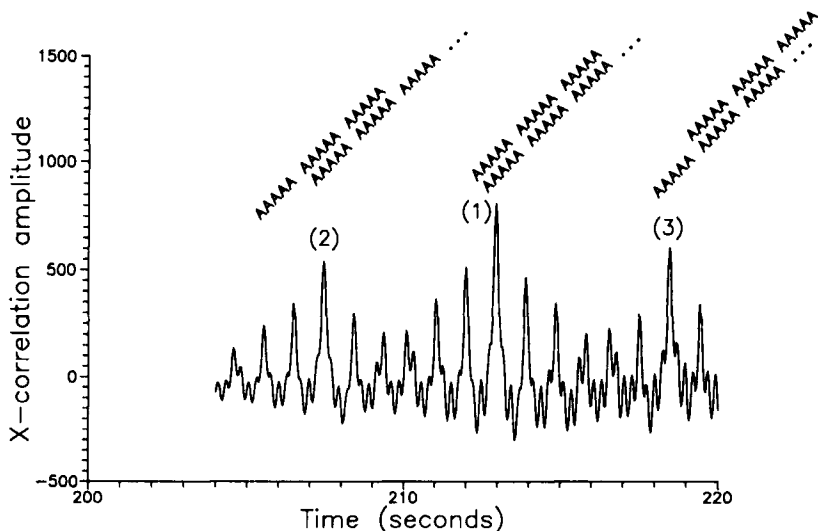


Fig 6—A convolution of the CW pattern for "AAAAA AAAAA AAAAA" with an identical model pattern without noise. The highest peak (1) shows the perfect match.

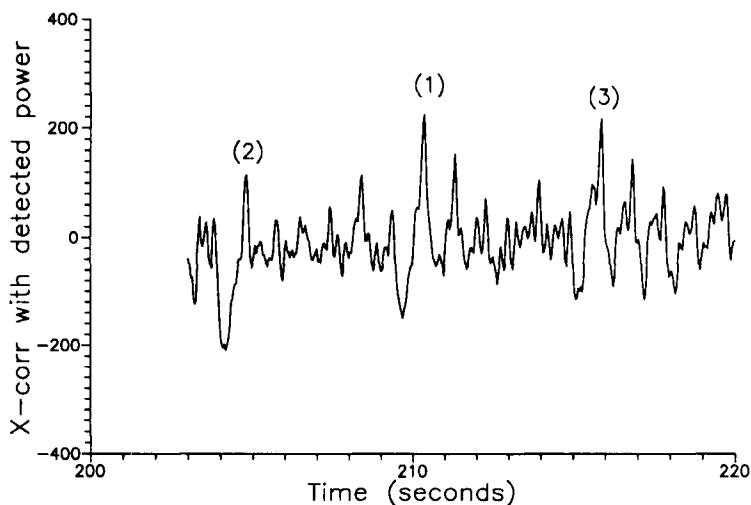


Fig 7—A convolution of ZRO level-A data with the CW pattern for "AAAAA AAAAA AAAAA." The peaks marked (1), (2) and (3) correspond to the similarly labeled peaks of the model data shown in Fig 6.

sending speed from 10 WPM in the first 5-digit group down to 9.95 WPM during the 3rd and last group. This may not seem like much, but it is enough to cause loss of synchronization with the timing of dots and dashes near the end of the data.

Finally, more trial cross-correlations were made taking this drifting CW speed into account. Correlations for each trial 5-digit number were calculated with additional time offsets in steps of 40 ms, over a 1-second interval. The revised candidate answers

were then listed in order of relative correlation magnitude. Fig 8 summarizes the results; the maximum correlation amplitude found for a given 5-digit number is plotted against the time at which that maximum correlation occurs. The best ~100 of the 100,000 trials are shown. It is encouraging to see that the strongest correlation occurs within a few milliseconds of the predicted start of the data. The most probable answers are also clustered at start times separated by intervals of 0.24 seconds, which is

the duration of a CW dot-space combination. The 5-digit number showing the highest correlation amplitude was submitted to WA5ZIB as the ZRO level-A report. There was a small celebration at AA7FV when Andy MacAllister confirmed that this was the correct number!

Other Applications

Moonbounce

One obvious application of these techniques is to low-power moon-bounce (EME) communication. For this to be successful, conventions need to be agreed on the detailed format of transmissions: the precise speed, timing, and the synchronization sequence (eg, CQ CQ CQ ..., or repeated call signs). It is essential to use machine-sent CW or other modulation. Although the processing described here has been for CW, similar techniques can be applied to most forms of modulation. An additional 3-dB gain in S/N with CW could be realized by using frequency-shift keying (FSK) instead of on-off keying. With signals buried so far in the noise, active error-correction modes, such as AMTOR, bring little gain in sensitivity on their own, but could be combined with these DSP algorithms. The gain in sensitivity achievable with the processing presented here depends on the exact circumstances (CW speed, etc), but is at least 10 dB when compared to the human ear alone.

OSCAR 13 Leakage Radiation

DSP algorithms were used in August 1993 to search for possible leakage radiation from the 436-MHz exciter of OSCAR 13. The Mode-JL downlink transmitter of AO-13 failed in May 1993.^{7,8} The cause of failure is not yet known, but if any weak signal from the Mode-JL exciter could be detected, for example via leakage through the defective power amplifier, this might help the understanding of the problem. During August 1993, the S-band beacon and the L-band beacon (ie, the L-band exciter) were both switched on simultaneously for part of AO-13's orbit (see Note 7). An unsuccessful attempt was made to detect low-level leakage from the Mode-JL exciter during these periods.

Data were recorded with the antenna pointed towards AO-13 and the Doppler-corrected 70-cm beacon frequency centered within the 2-kHz receiver passband. More than 850 power spectra, with 8-Hz frequency sampling and covering ~100 seconds of raw data,

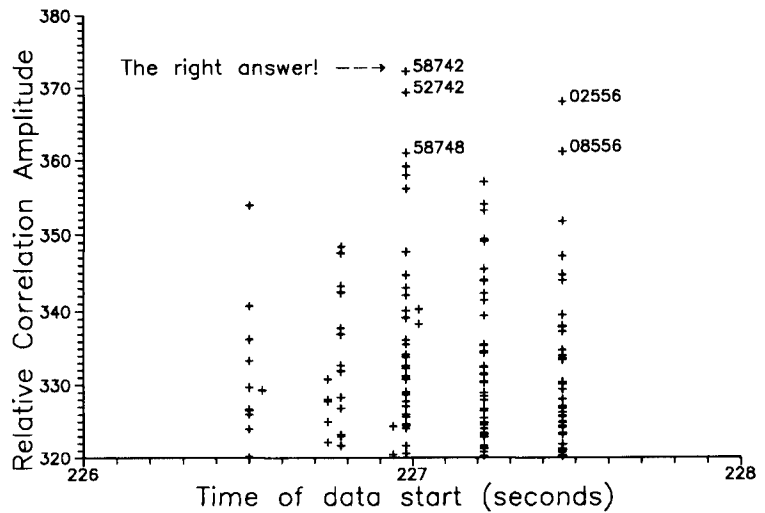


Fig 8—Relative correlation of the most likely matches of different 5-digit numbers to the ZRO level-A data. The predicted start time is 227.0 s; correlations were computed every 0.04 s from 226.5 to 227.5 s.

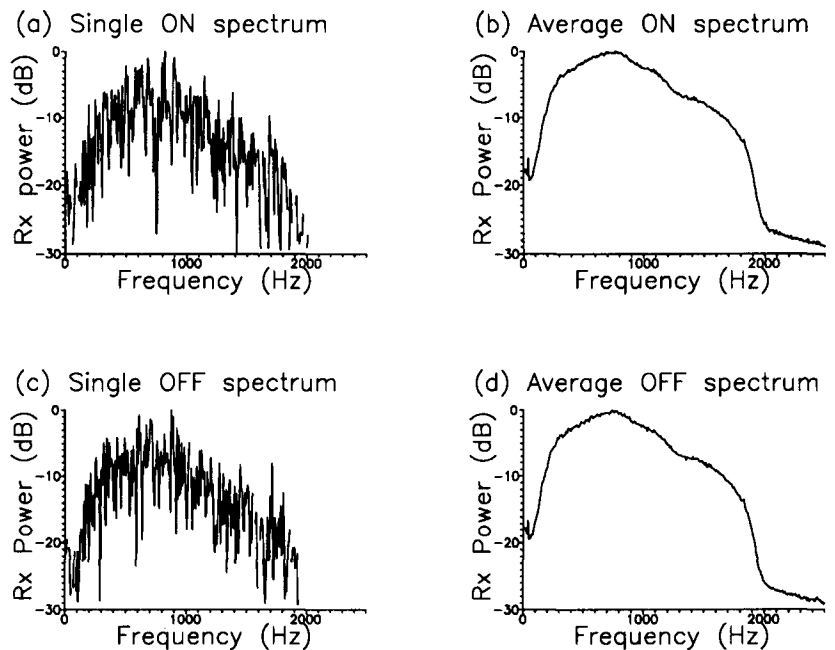


Fig 9—A comparison of the receiver noise-power spectrum looking at OSCAR 13 with similar spectra looking at blank sky. All spectra have a frequency resolution of 8 Hz. Spectrum (a) is derived from 0.125 seconds of data and is dominated by random noise. (b) shows the result of average 852 such spectra, allowing for changes in Doppler frequency; the random noise has been reduced dramatically. (c) shows a single spectrum looking away from the satellite, with (d) showing the average of 868 such spectra. Any weak emission from OSCAR 13 would show up as small differences between the average ON (b) and OFF (d) spectra.

were generated using the FFT algorithm. An example spectrum is shown in Fig 9(a); it is dominated by random noise. Each spectrum was individually shifted in frequency to allow for the Doppler drift of ~0.3 Hz/second. These

Doppler-corrected spectra were then averaged together giving a combined spectrum which showed the receiver noise passband with any possible additional energy from AO-13 superimposed; an example of the average spec-

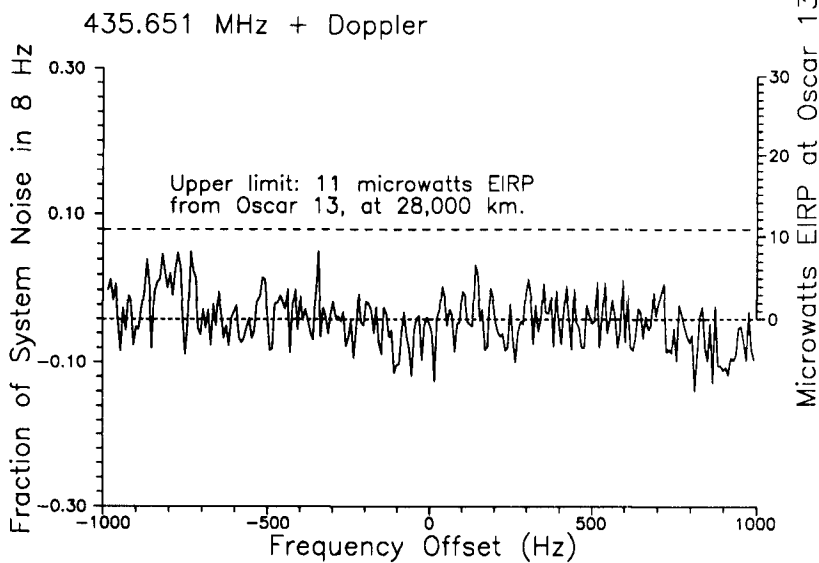


Fig 10—A spectrum of the radiation at 436 MHz from AO-13, when the Mode-JL exciter was turned on and should have been sending RTTY. Maximum leakage radiation from AO-13 is less than 11- μ W EIRP in any 8-Hz band.

trum is shown in Fig 9(b). The overall receiver passband shape is shown very clearly. A similar spectrum, generated from data taken with the antenna looking at blank sky, was also generated. Figs 9(c) and 9(d) show a single-component OFF-satellite spectrum and the corresponding average spectrum. In both averaged spectra, the random noise has been reduced by the square root of the number (~850) of spectra averaged together. Any weak emission from OSCAR 13 would show up as slight differences in the ON-satellite and OFF-satellite spectra. The two averaged spectra were subtracted and the spectrum difference was normalized to give uniform sensitivity across the 2-kHz passband, calibrated as a fraction of receiver system noise. This analysis removes frequency-dependent offsets and gain variations in the spectrum, which result mainly from ripples and slopes in the receiver IF passband. The final result is shown in Fig 10. There is a small residual dc offset of about -4% of the average system noise, which is consistent with a gain change of ~0.2 dB between the observations on AO-13 and on blank sky. The intention is to search for a narrowband emission from AO-13, so this offset is unimportant. The raw data had been recorded while AO-13 should have been sending

RTTY, so leakage radiation would appear as a pair of spikes in the spectrum, separated by the FSK shift of 170 Hz. No such signals are seen with an upper limit (3 times the RMS noise along the spectrum) equal to 12% of the system noise within any 8-Hz band. For this experiment the total system noise temperature was believed to be 140 K, and the antenna gain 14.5 dB; these values were confirmed by careful observations of solar noise. The upper limit can then be calibrated in terms of EIRP from the satellite, which was at a range of 28,000 km; details of the calculation are given in the Appendix. The corresponding limit for leakage radiation from AO-13 is *less than 11 microwatts EIRP in any 8-Hz band*. For an RTTY transmission, power is on average split equally between the two FSK tones and the modulation sidebands. Allowing for this, the maximum *total EIRP* from AO-13 is *less than 44 microwatts*. Several additional spectra similar to Fig 10 were produced, covering a total frequency span of ± 2 kHz from the expected beacon frequency, allowing for Doppler shift. No significant emission from AO-13 was found in any of these spectra to the same upper limit of 11 μ W EIRP in any 8-Hz band. There are always uncertainties and errors in measurements like this, but it is rea-

sonably certain that the total 70-cm leakage radiation from AO-13 must be well below 100 μ W EIRP.

The sensitivity to narrow-band radiation could be improved with longer averaging times, or, if the receiver had been sufficiently stable, by using higher selectivity than the 8 Hz used here. The overall frequency stability of receivers and transmitters may limit the ultimate sensitivity attainable.

Summary

This article has shown the application of some DSP techniques to the recovery of very weak CW from OSCAR 13, giving 100% copy of the ZRO level-A test at 30 dB below the AO-13 beacon. The procedure can allow reception of signals very much weaker than the background noise level, and gives 10 dB or more advantage over the human ear. Although the example given is for CW, similar techniques are applicable to other modes of modulation. Finally, by averaging power spectra together, DSP algorithms have been used to set a limit of less than 44 μ W EIRP for the total leakage radiation through the defective 436-MHz power amplifier from OSCAR 13 at a range of 28,000 km. With longer averaging times, and if the receiver and transmitter are sufficiently stable, higher frequency resolution could improve the sensitivity to narrow-band signals even further.

All the analysis so far has been carried out off-line. A future project is to adapt the algorithms and software to real-time processing and display.

Notes

- ¹MacAllister, Andrew C., WA5ZIB, "The AMSAT Awards Program," *Proceedings of the AMSAT-NA Tenth Space Symposium*, p 197. Published by ARRL, October 1992.
- ²*Amsat News Service Bulletin ANS-184.02*, July 2, 1993.
- ³Smith, Gould, WA4SXM, "DSP and the Average Satellite Operator," *Proceedings of the AMSAT-NA Tenth Space Symposium*, p 88. Published by ARRL, October 1992.
- ⁴Press, W.H., Flannery, B.P., Teukolsky, S.A. and Vetterling, W.T. "Numerical Recipes," *Cambridge University Press*, 1986.
- ⁵Vetterling, W.T., Teukolsky, S.A., Press, W.H. and Flannery, B.P., "Numerical Recipes Example Book (FORTRAN)," *Cambridge University Press*, 1985.
- ⁶"Coherent CW," *ARRL Handbook*, 65th Edition, p 21-15 to 21-17. Published by ARRL, 1988.
- ⁷Miller, James, G3RUH, *AO-13 Transponder Schedule*, broadcast over the Internet and elsewhere, June 10, 1993.
- ⁸Miller, James, G3RUH, "Managing OSCAR 13," *Proceedings of the AMSAT-NA Eleventh Space Symposium*, p 46. Published by ARRL, October 1993.

Appendix: Calculation of EIRP from OSCAR 13

The upper limit of antenna temperature from radiation from AO-13 is 12% of the receiver system noise:

$$T_a < 0.12 \times T_{sys}$$

Measurements on the receiver, and of solar noise, give:

$$T_{sys} \approx 140 \text{ K}$$

so that

$$T_a < 16.8 \text{ K}$$

The power picked up in area A by the antenna, with bandwidth $B=8 \text{ Hz}$, and $k = \text{Boltzmann's constant} = 1.38 \times 10^{-23}$ is:

$$P_r = k \cdot T_a \cdot B \\ = 1.38 \times 10^{-23} \times 16.8 \times 8 = 1.85 \times 10^{-21} \text{ W}$$

This corresponds to a voltage V at the receiver terminals of

$$V \approx 0.0003 \mu\text{V in } 50 \Omega$$

The wavelength λ at 435.651 MHz is 68.8 cm.

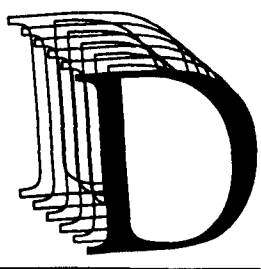
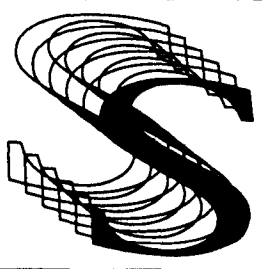
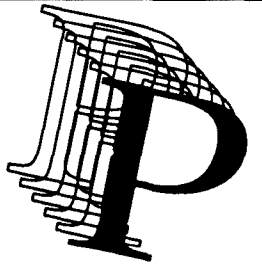
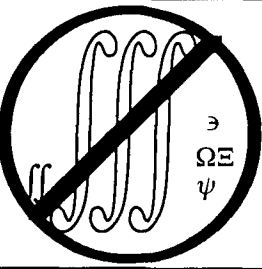
The antenna gain is 14.5 dBd, $\sim 16.5 \text{ dBi}$, or $G=44.7$. The capture area A of the antenna is:

$$A = \frac{G \cdot \lambda^2}{4 \cdot \pi} = 1.68 \text{ m}^2$$

The total effective power P radiated from OSCAR 13, at a distance $D=28,000 \text{ km}$ is then:

$$P < P_r \cdot \frac{4 \cdot \pi \cdot D^2}{A} = 10.8 \times 10^{-6} \text{ W} \\ P < 11 \mu\text{W}$$

□□

		
Without Tears™	Learn DSP and Put your Knowledge to work Immediately!	
Coming to a Place Near You Ft. Lauderdale Albuquerque Washington D.C. Chicago, Dallas San Jose, Long Beach	Call 7 Domain Technologies, Inc. (800)-967-5034 (404)-664-6738 Call 9-5 EST. Ask for brochure. Our 2-Day Advanced Course is ready. Call for info	By Taking This 3-Day Course You will really learn DSP. Guaranteed!

Surface Mount Chip Component Prototyping Kits—
Only **\$49.95**
INDIVIDUAL VALUES AVAILABLE



CC-1 Capacitor Kit contains 365 pieces, 5 ea. of every 10% value from 1pf to 33µf. CR-1 Resistor Kit contains 1540 pieces: 10 ea. of every 5% value from 100Ω to 10 megΩ. Sizes are 0805 and 1206. Each kit is ONLY \$49.95 and available for immediate One Day Delivery!

Order by toll-free phone, FAX, or mail. We accept VISA, MC, COD, or Pre-paid orders. Company PO's accepted with approved credit. Call for free detailed brochure.

COMMUNICATIONS SPECIALISTS, INC.
426 West Taft Ave. • Orange, CA 92665-4296
Local (714) 998-3021 • FAX (714) 974-3420
Entire USA 1-800-854-0547

Want to reap the rewards of teaching ham radio? Ask ARRL Educational Activities Department for *your* free package on teaching youth or adults.

Zack Lau, KH6CP/1

Designing a 2-Meter Power Amplifier

I got an interesting request: someone wanted a book that would help them design antennas, but one that would do so without presenting any completed designs. In a way, this request makes sense; design is something you learn by doing, rather than by reading about completed designs. Of course, the usual problem is that the areas authors get fuzzy about are the tough parts of the design—the parts you need to get right to get it to work—rather than the straightforward stuff a beginner can tackle. In the spirit of letting the reader *do* design, rather than just read about it, this month I've decided to let you complete the design I've started (a 2-meter power amplifier). I'm pretty sure I've converted the problem into a straightforward textbook exercise, rather than an indoctrination into the "black magic" of RF. But I'll also highlight two challenges for the experts to tackle.

One of the most common amateur amplifier design techniques is to take a design from a data book and modify it for use in the nearest amateur band. One such design, described in a recent article, uses the MRF137, a Motorola TMOS FET.^{1,2} This approach has its dangers, however. A close reading of the article and an analysis of the stability of the circuit reveal that it can quite easily become an oscillator, instead of an amplifier. Perhaps the circuit from the data sheet wasn't the best one to copy.

¹Cunningham, J, AA4AW, "A 2 Meter FET Amplifier for Your Handheld," 73, Oct 1992, pp 20-24.

²Motorola RF Device Data Volume 1, Fifth Edition, First Printing, 1988, p 2-378.

225 Main Street
Newington, CT 06111
email: zlau@arrl.org (Internet)

Looking at the MRF137 data sheet shows that the chosen circuit was designed to maximize both gain and drain efficiency by not wasting any power in feedback loops or shunt resistances. The circuit was optimized for showing how well the transistor *can* work as an amplifier, not how it is best configured as a practical, stable amplifier.

By making an amplifier stable, I am referring to a design that will not oscillate, no matter what impedances the input and output are terminated with. The most critical frequencies in stability analysis are those far away from the design frequency, since most amateurs take great care in making sure that everything is adjusted for a low SWR *at the operating frequency*. Thus, in-band, the terminations are usually quite good. Intuitively, you would expect good stability with good terminations—power from the amplifier just disappears into the terminations. On the other hand, power reflected from poor terminations might be expected to reinforce oscillations, if returned with the proper phase. Looking at stability from a designer's standpoint, you might consider an unconditionally stable sub-circuit as a useful building block. Even if the design impedances aren't 50 ohms, you can match them however you wish without having to worry about making the amplifier unstable. This is a popular technique: dividing a difficult problem into several simpler problems.

Fig 1 shows a revised MRF137 amplifier, which includes a few added refinements to make the amplifier more practical. First, I added a drain-to-gate feedback resistor for stability. According to computer simulation, reasonable amounts of parasitic reactance within this feedback path—such as that from the inductance inherent in real resistors—do not noticeably affect either the performance at 2 meters or the stability across the spectrum.

Next, since I was interested in devel-

oping a no-tune amplifier, I raised the input impedance by inserting a series resistor, rather than using an L-C step-up network. An L-C step-up network would tend to produce more gain, though how much one can get depends on the stability or lack thereof of the transistor. But such an efficient network would also complicate the design by increasing the interaction between the input and output networks, which is one of the disadvantages of shunt feedback. Computer modeling is probably the only practical way for most amateurs to design stable amplifiers—though it's possible to achieve stability on the bench with some rather exotic test equipment.

The modeling was done at a higher supply voltage than that actually used. The MRF137 is nominally a 28-volt device, and that is the supply voltage for which computer models of the device are available. I wanted to run the circuit from a voltage-doubler power supply with a 12-volt input. This gives only about 23 volts for the supply. Using a higher supply voltage for the analysis usually means that the predicted gain is a few dB higher than is actually realized at the lower voltage. The predicted stability also tends to be worse than actual when this is done, though there are undoubtedly exceptions. By the way, since stability analysis is done using a small-signal model, you might wonder how applicable it is to a power amplifier, which is sometimes used in a nonlinear fashion. Usually, it does quite well, because stability is often enhanced by the gain compression encountered under large-signal conditions.

Though unconditional stability is pretty well defined with respect to linear amplifiers like this one, it gets more complex for class-C amplifiers. Bench testing for stability is a tedious process. How can you test for instability under varying source and load conditions at particular frequencies? If I were looking to cause trouble, I'd

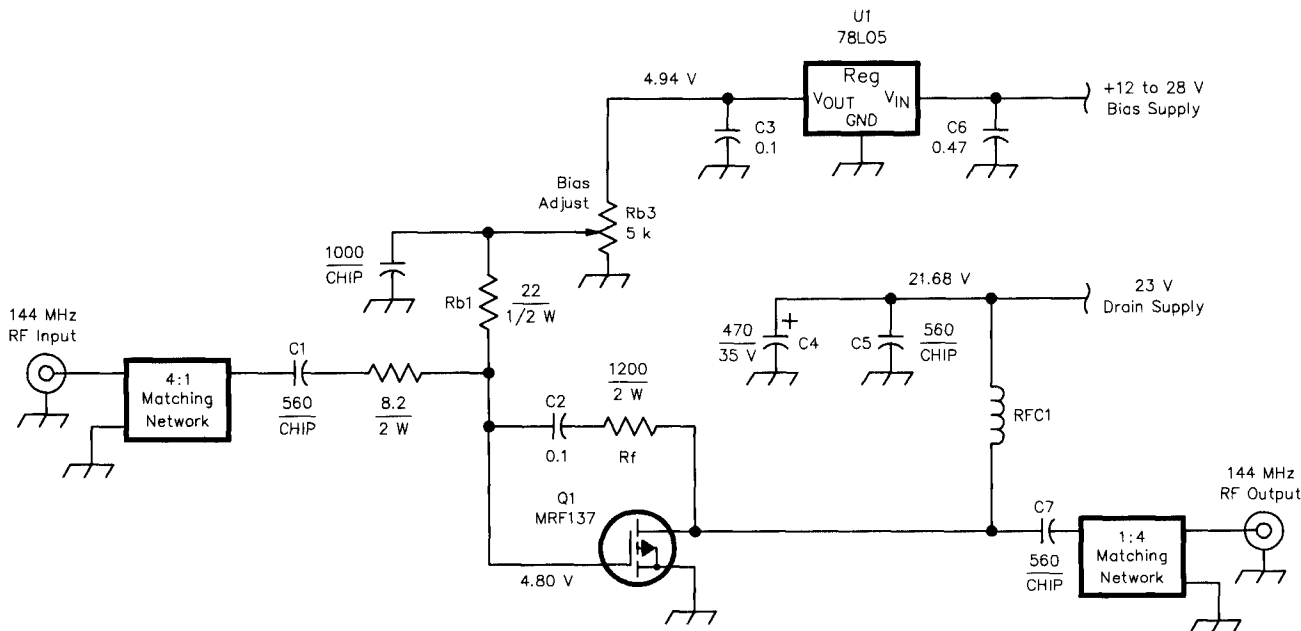


Fig 1—Schematic of the almost-completed 2-meter amplifier. You supply the matching networks! (Note that the measured drain supply voltage is a bit less than the nominal 23 volts.)

C1—A leaded capacitor may be used if its series inductance is 5 nH or less.

C6—An electrolytic capacitor of equal or greater value may be used here. Install with proper polarity.

Q1—MRF137 power transistor. Mount on a suitable heat sink. (Pages 6-20 to 6-23 of the *ARRL Handbook* describe heat sink design.) For SSB/CW contesting, a 3° C/watt heat sink works fine.

Rb2—5-k Ω , 10-turn trimmer potentiometer. I had no problems using a 10-k Ω pot. However, 5 k Ω will result in a regulator load of 1 mA, which is the minimum load over which the regulated voltage is specified in the *National Data Power IC's Databook*, 1993 Edition (page 1-198).

Rf—Feedback resistor, 1200 Ω , 2 W. Up to 50 nH of series inductance in this loop should cause no problems. Metal-

oxide film resistors work just fine. Do *not* use a wirewound resistor here. RFC1—11 turns no. 20 enameled wire, close wound, with 0.19-inch inside diameter.

U1—78L05 5-volt regulator IC. A less common 78L08 8-volt regulator would accommodate variations in gate threshold voltage, which range from 1 to 6 volts, for 25 mA of drain current, with the MRF137.

probably start measuring such an amplifier with a sharp filter, such as a tuned cavity, on the input and an unterminated output. I'd then vary the lengths of the input and output lines to present a variety of source and load impedances. Oscillations are detectable by sharp jumps in the dc supply current as the input power is varied. A spectrum analyzer, used as a broadband receiver, will do even better, if you have one available. I'd also guess that the worst-case input level was that which gave maximum gain—the point on the output-versus-input curve with the steepest slope. At low input levels, the gain of the amp is often less than 1 (that is, less than 0 dB), while at high input levels you might expect the amplifier to injection-lock onto the input signal. Worst-case stability is therefore usually between these levels.

A current-limited supply is essential for stability measurements, as is a good heat sink. Otherwise, you might end up replacing expensive RF transistors. If you are trying to stabilize a

commercial product, you might consider getting a fan to help out the existing heat sink by blowing air across it. If you have a choice of transistors, you should look for one rated to withstand a 20- or 30-to-1 mismatch on the output.

Your Turn

Your job is to design the input and output networks. The input network has to convert the transistor input circuit impedance from 12.5 ohms to 50 ohms, while the output network should convert 50 ohms to the impedance necessary to obtain a clean 10 watts of output. Ten ohms with a few ohms of capacitive reactance is probably a good starting point. Perhaps the most straightforward way is with L-C step-up networks, which you will undoubtedly have to tune for proper performance. Air-dielectric trimmer capacitors have the lowest loss, while mica-dielectric capacitors also do quite well at VHF. Plastic-film capacitors *aren't* recommended.

The astute reader will notice that I didn't say you should match the transistor output impedance to 50 ohms. Unfortunately, as in noise matching, the optimum load impedance is often different from that obtained by conjugate matching. Typically, you determine this by first calculating the resistance for optimum power transfer, based on the supply voltage and the desired power output. (Actually, you might fudge the power output value, since a linear amplifier typically works a lot better at half the maximum power output.) Next, you might apply a correction based on the parasitic reactances of the device, such as the output capacitance. Most important, realize that this is just a starting value, subject to change depending on how well the amplifier works!

With the proper networks, you should see about 10 watts output for 2 watts input, with intermodulation distortion (IMD) products down at least 40 dB when biased at 1 amp. 0.5 amps of bias current is probably more reasonable, except that I wanted

the signal to be as clean as practical. A low pass filter of at least 5 elements is suggested to meet FCC spectral purity requirements. If you get stuck, an sase will get you a schematic of the input and output networks I used, though you will have some difficulty getting the parts.

Haven't Had Enough?

Use of broadband matching networks or transformers for input and output matching are also a possibility, though this may be too much of a challenge. The input impedance ratio is a convenient 4:1, which means a transmission-line transformer would work

well if you had 25 Ω -coax. And paralleling coax theoretically would work, although it might not really be practical. On the other hand, I've not found a suitable broadband output matching circuit, even using exotic parts. I've seen several push-pull examples of VHF amplifiers with broadband matching, but I don't recall any single-ended examples. At microwaves, it might make more sense just to tweak the output lines for maximum output, rather than bothering with calculations. This is particularly true of devices which you know little about, such as FETs optimized for frequencies you aren't interested in.

A real challenge would be to design a high-efficiency, low-noise 28-volt power supply that runs from 12 volts. Ideally, it would monitor the input RF signal to determine the optimum bias current. A simpler task is to just design a high-efficiency voltage doubler. You might wonder—why not just run the amplifier directly from 12 or 14 volts, instead of bothering with a voltage converter? The most serious reason is the increase in 3rd-order IMD—it can go from excellent to poor (better than -40 dBc to worse than -30 dBc). In addition, the gain generally drops, though this often isn't a problem at lower frequencies. \square

Join the FUN on the

SATELLITES

YES! Anyone with a Technician Class license or higher can work the



via the
OSCARS

Learn how: Join AMSAT today!

For a limited time, new members receive :

ORBITs - Tracking software for IBM compatible computers by W0SL

How to Use the Amateur Satellites - A great book by KB1SF

write or call



AMSAT

**PO Box 27 Washington, DC 20044
301-589-6062**

CAPMANtm

SKYWAVE ANALYSIS

"Use IONCAP⁺ like a pro!"

YOU GET

CAPMAN - Menu driven input & control with context-sensitive help at a mouse click!

Multicolor - Output Graphics display!
Extra or Novice, its EASY to use!

IONCAP⁺ - the same 32 bit tool the pros use to get S/N, MUF, FOT, LUF, Reliability and much More! Special Long-distance model for DXers!

MININEC & ELNEC interface for your custom antenna input!

INCLUDE your contacts & friends in the contact library of 494 prefixes!

Entire CAPMAN package -- \$89
USA postage paid. Overseas add \$3.50

Order right away from:

LUCAS Radio/Kangaroo Tabor Software
2900 Valmont Rd, Suite H
Boulder, CO 80301

(303) 494-4647 (494-0937 fax)

VISA MC CHECK MONEY ORDER

Upcoming Technical Conferences

West Coast VHF Conference

April 29-May 1, 1994, Sheraton Hotel in Cerritos, California.

For more information, contact:
Gracey Hastings, KK6CG, and
Bob Hastings, K6PHE
854 Bernard Drive
Fullerton, CA 92635.

Central States VHF Conference

July 29-30, 1994, Wilson World Hotel, Memphis, Tennessee

Contact:
Dave Meier, N4MW
3205 Covington Pike
Memphis, TN 38128
tel 901 382-4912.

Microwave Update '94

Will be held sometime after Labor Day, in Estes Park, Colorado.

Contact:
William McCaa, NØRZ
PO Box 3214
Boulder, CO 80307.

1994 ARRL Conference on Digital Communications

A definite date has not been set at this time, however an August time-frame is being planned. It will be held in the Minneapolis/St. Paul area. The event is being sponsored by the TwinsLAN ARC.

Contact:
Carl Estey, WAØCQG
276 Walnut Lane
Apple Valley, MN 55124,
tel 612 432-0699.

Internet:
estey@skylar.mavd.honeywell.com;
packet:
WACQG@WACQG.#MSP.MN.USA.NA.

Call for papers: Anyone interested in digital communications is invited to submit a paper(s) for this conference. Papers can be on any aspect of digital communications. The deadline for receipt of papers is June 20, 1994. Papers can be in electronic or camera-ready form, and should be sent to:

Maty Weinberg
ARRL
225 Main Street
Newington, CT 06111
Internet: lweinber@arrl.org.

Contact:
John Sorter, KB3XG
5290 Stump Road
Pipersville, PA 18947.

Eastern States VHF Conference

A date has not been set at this time.

Contact:
Stan Hilinsky, KA1ZE
17 Pilgrim Drive
Tolland, CT 06084
tel 203 649-3258 (W)
203 872-6197 (H).

Pack Rats Conference

A date has not been set at this time, although it's usually the first Saturday in October.

(Have an upcoming technical event? Drop us a note with the all the details and we'll include it in Upcoming Technical Conferences.)

QEX Subscription Order Card

American Radio Relay League
Newington, CT USA 06111-1494

QEX, The ARRL Experimenter's Exchange is available at the rates shown at left. Maximum term is 12 issues, and because of the uncertainty of postal rates, prices are subject to change without notice.

For 12 issues of QEX in the US

- ARRL Member \$12.00
 Non-Member \$24.00

In Canada, Mexico and US by First Class Mail

- ARRL Member \$25.00
 Non-Member \$37.00

Elsewhere by Airmail

- ARRL Member \$48.00
 NonMember \$60.00

Remittance must be in US funds and checks must be drawn on a bank in the US. Prices subject to change without notice.

Renewal New Subscription

ARRL Membership Control # _____

Name _____ Call _____

Address _____

City _____ State or Province _____ Postal Code _____

Payment Enclosed

Charge
 MasterCard VISA American Express Discover

Account # _____ Good thru _____

Signature _____

Date _____